

AMERICAN UNIVERSITY OF BEIRUT

INTENSIFYING CARBON CAPTURE USING A SMALL,
FLEXIBLE, AND LOW-COST REACTOR

by

LYNN ANTOINE KAADY

A thesis
submitted in partial fulfilment of the requirements
for the degree of Master of Science
to the Department of Chemical and Petroleum Engineering
of the Maroun Semaan Faculty of Engineering and Architecture
at the American University of Beirut

Beirut, Lebanon

December 2018

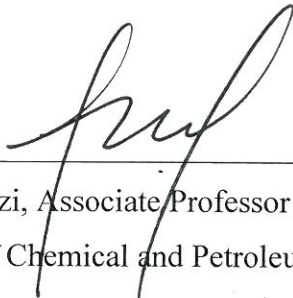
AMERICAN UNIVERSITY OF BEIRUT

INTENSIFYING CARBON CAPTURE USING A SMALL,
FLEXIBLE, AND LOW-COST REACTOR

by

LYNN ANTOINE KAADY

Approved by:



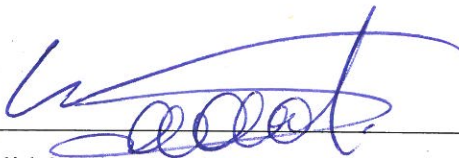
Dr. Fouad Azizi, Associate Professor
Department of Chemical and Petroleum Engineering

Advisor



Dr. Mahmoud Al-Hindi, Associate Professor
Department of Chemical and Petroleum Engineering

Member of Committee



Dr. Walid Saad, Associate Professor,
Department of Chemical and Petroleum Engineering

Member of Committee

Date of thesis defense: December 12, 2018

ACKNOWLEDGMENTS

I would like to thank and express deep gratitude and appreciation to my thesis advisor Prof. Fouad Azizi for his constant help, support and guidance all throughout the past year.

Special thanks to Prof. Mahmoud Al-Hindi and Prof. Walid Saad for being members of my thesis committee.

Finally, I would also like to thank to my family members, my mother, father and brother, and my friends for their daily support, motivation and encouragement.

AN ABSTRACT OF THE THESIS OF

Lynn Antoine Kaady

for

Master of Science

Major: Chemical Engineering

Title: Intensifying carbon capture using a small, flexible and low-cost reactor

Carbon capture is one of the means for mitigating the impact of greenhouse gas emissions. Several carbon capture methods are available, the most promising of which appears to be that involving a chemical reaction. This study attempts to intensify the chemical absorption of carbon dioxide into an aqueous solution of sodium hydroxide using a novel reactor equipped with a new type of static mixers.

The efficiency of the reactor in removing carbon dioxide was determined by quantifying the volumetric mass transfer coefficient (k_{LA}), CO₂ removal efficiency, and specific energy consumption as a function of various process parameters. These include gas and liquid flow rates and mixer geometry. The volumetric mass transfer coefficient and efficiency were found to increase with liquid superficial velocity and gas volume fraction up to 1.3563s⁻¹ and 98%, respectively. Additionally, it was found that the screen geometry greatly affects the mass transfer operation whereby the screens having smaller open area yielded the highest k_{LA} values. In this investigation, k_{LA} values were found to be comparable and even higher than other gas/liquid contactors used for the CO₂ chemisorption into NaOH, namely, bubble columns, packed beds and rotating packed beds.

CONTENTS

ACKNOWLEDGEMENTS	i
ABSTRACT.....	ii
LIST OF ILLUSTRATIONS.....	vii
LIST OF TABLES.....	viii

Chapter

I. INTRODUCTION	1
II. LITERATURE REVIEW	7
A. Chemical absorption using amine-based and carbonate-based systems...	7
B. Chemical absorption of CO ₂ into NaOH in different reactors.....	10
III. Experimental Section.....	15
A. Reaction of CO ₂ with aqueous NaOH.....	15
B. Experimental Setup	16
C. Method of analysis	21
1. Estimation of the overall volumetric mass transfer coefficient.....	21
a. Concentration of CO ₂ in the liquid phase at equilibrium with the gas phase.....	22
b. Estimation of the overall volumetric mass transfer coefficient.....	23

2.Efficiency	25
3.Power Consumption	25
IV. RESULTS AND DISCUSSION	28
A. Pressure drop	28
B. Volumetric mass transfer coefficient	30
1.Effect of liquid flow rate	31
2.Effect of gas holdup	32
3.Effect of Reynolds number.....	33
C. Efficiency	35
D. Energy requirements	39
E. Correlating the volumetric mass transfer coefficient.....	41
F. Comparison with other gas-liquid contactors used for carbon capture.....	42
V. CONCLUSION AND RECOMMENDATIONS.....	44
Appendix	
I. SUPPLEMENTARY FIGURES	58
II. RAW DATA FROM EXPERIMENTS	62
III. SAMPLE CALCULATION	71
IV. ERROR ANALYSIS	76

NOMENCLATURE

a	Interfacial area of contact	$[\text{m}^2/\text{m}^3]$
b	Screen wire diameter	$[\mu\text{m}]$
$(C_{\text{CO}_2})^*$	Concentration of CO_2 at equilibrium with the gas phase	$[\text{mol}\cdot\text{L}^{-1}]$
D	Pipe diameter	$[\text{m}]$
E	Energy dissipation rate	$[\text{kW}]$
E_{spm}	Specific energy consumption rate per unit mass of liquid processed	$[\text{kWh}/\text{kg}]$
H_{CO_2}	Henry's law constant in an electrolyte solution	$[\text{mol}\cdot\text{bar}^{-1}\cdot\text{L}^{-1}]$
k_L	Liquid side mass-transfer coefficient	$[\text{m}\cdot\text{s}^{-1}]$
$k_L a$	Volumetric mass transfer coefficient	$[\text{s}^{-1}]$
L	Inter-screen spacing in the mixing section	$[\text{m}]$
M	Wire mesh size	$[\text{m}]$
Mn	Mesh number	$[-]$
P_{CO_2}	Partial pressure of CO_2	$[\text{atm}]$
Q	Volumetric flow rate	$[\text{m}^3/\text{s}]$
R	Gas constant	$[\text{atm}\cdot\text{L}\cdot\text{mol}^{-1}\cdot\text{K}^{-1}]$
Re	Empty pipe Reynolds number, $\frac{\rho U_T D}{\mu}$	$[-]$
Re_b	Wire Reynolds number, $\frac{\rho U_T b}{\mu}$	$[-]$

Re_M	Mesh Reynolds number, $\frac{\rho U_T M}{\mu}$	[-]
Re_j	Individual-jet Reynolds number, $\frac{\rho U_T}{\mu \alpha} \frac{2(M-b)}{\sqrt{\pi}}$	[-]
Re_{jet}	Macroscopic jet Reynolds number, $\frac{\rho U_T D}{\alpha \mu}$	[-]
t	Residence time	[s]
T	Temperature	[K]
U	Superficial velocity	[m/s]
V	Volume	[L]

Greek Symbols

α	Percentage open area of screen	[%]
ΔP	Pressure drop in the pipe	[Pa]
ε	Turbulent kinetic energy dissipation rate	[W/kg]
ρ	Density	[kg/m ³]
φ	Gas holdup	[%]

Subscripts

g	Gas
L	Liquid
T	Total
mix	Mixture properties

ILLUSTRATIONS

Figure	Page
1. Schematic Representation of the experimental setup (1): supply tank (2): drain tank (3):NaOH tank (4):centrifugal pump (5): dosing pump (6): samples extracted for analysis (7): pressure sensors.....	14
2. Reactor Internals.....	14
3. Screen-type static mixer.....	15
4. Pressure drop for four different screen geometries versus: (a) Empty pipe Reynolds number, Re_{pipe} and (b) Wire Reynolds number, Re_b for $\Phi = 0\%$...	23
5. Effect of gas holdup on the pressure per screen: (a) pressure drop versus..... superficial velocity of gas – liquid mixture and (b) pressure drop versus liquid velocity for $Mn = 80$	24
6. Effect of Superficial velocity and gas holdup on kLa :(a) $Mn = 30$, (b) $Mn = 50$, (c) $Mn = 80$ and (d) $Mn = 100$	25
7. The variation of kLa with the various Reynolds numbers for all four screen geometries for $\phi = 30\%$: (a) Re , (b) Re_b , (c) Re_M , (d) Re_j and (e) Re_{jet}	28
8. Effect of mesh geometry on efficiency at 1.6 m/s and $\Phi = 10\%$	29
9. Effect of total superficial flow rate on efficiency for $Mn = 80$ and $\Phi = 30\%$	30
10. Effect of gas holdup on efficiency for $Mn = 80$ and $UT = 1.6$ m/s	30
11. Effect of Superficial velocity and gas holdup on Efficiency:(a) $Mn = 30$, (b) $Mn = 50$, (c) $Mn = 80$ and (d) $Mn = 100$	31
12. kLa versus the energy needed to process a unit of the flowing mixture, E_{spm} , : (a) $Mn = 30$, (b) $Mn = 50$, (c) $Mn = 80$ and (d) $Mn = 100$	33
13. Effect of gas holdup and superficial liquid velocity on the pressure drop per screen: (a) Mesh 30, (b) Mesh 50 and (c) Mesh 100.....	46
14. Effect of gas holdup and total superficial velocity on pressure drop per screen: (a) Mesh 30, (b) Mesh 50 and (c) Mesh 100.....	47
15. The variation of kLa with Reynolds number for all four screen geometries ($\phi = 10\%$): (a) Re_{pipe} , (b) Re_b , (c) Re_M , (d) Re_j and (e) Re_{jet}	48

16. The variation of $k_L a$ with Reynolds number for all four screen geometries ($\varphi = 20\%$): (a) Repipe, (b) Reb, (c) ReM, (d) Rej and (e) Rejet.....	49
17. $k_L a$ calculation.....	62

TABLES

Table	Page
1. Characteristics of the investigated stainless-steel plain weave wire meshes.....	15
2. Operating Conditions.....	16
3. Ion Contribution values.....	19
4. Summary comparison between conventional reactors.....	33
5. Experimental Conditions.....	59
6. Ionic Strength calculation.....	61
7. Errors associated with the physical quantities.....	63
8. Sample calculation of the error on $U_T = 2$ m/s.....	64
9. Sample calculation of the error on φ for the condition $Mn = 30$, 1m/s & 20% Holdup.....	65
10. Calculation of the error on t for the condition $Mn = 30$, 1m/s & 20% Holdup	65
11. Estimation of the % error on Efficiency for the condition $Mn = 30$, 1m/s & 20% Holdup.....	67
12. Estimation of the % error on Reynolds number for the condition $Mn = 30$, 1m/s & 20% Holdup.....	68
13. Estimation of the % error on Efficiency for the condition $Mn = 30$, 1m/s & 20% Holdup.....	69

CHAPTER I

INTRODUCTION

The ability to reduce greenhouse gas (GHG) emissions is of utmost importance due to its direct impact on global warming. Carbon dioxide emitted from fossil fuel combustion, cement production and other industrial processes account for about 70 percent of the total greenhouse gas emissions (Olivier et al., 2017; UNEP, n.d.). According to various studies, CO₂ emissions are expected to further increase in the coming years (Olivier et al., 2017). Therefore, much attention should be dedicated towards developing more efficient carbon dioxide capture processes.

Carbon dioxide capture can be implemented both pre-, and post-, combustion. In these processes, the technology selection is dictated by the capital and operating cost of the process which largely depend on the partial pressure of CO₂ in the gas stream, solvent regeneration, efficiency of CO₂ removal and cost of additives required to overcome corrosion (Olajire, 2010). While both capture technologies could be retrofitted to existing plants, the pre-combustion method remains costly, as its capital and operating costs exceed that of post-combustion, therefore, most efforts are invested in the latter technology (Olajire, 2010). This is clearly highlighted in the large number of investigations that can be found in the open literature (Chiang et al., 2017; Duss et al., 2001; Koronaki et al., 2017; Kothandaraman et al., 2009; Niu et al., 2009; Samanta et al., 2012; Wang et al., 2013; Yang et al., 2008; Yoo et al., 2013). There exist several methods for post-combustion CO₂ capture. These include membrane separation (Powell and Qiao, 2006; Shekhawat et al., 2003), adsorption (Kato et al., 2005; Xu et al., 2005), and absorption (Aroonwilas et al., 1999; Chen et al., 2014, 2008; Chiang et al., 2017; Drăgan, 2016; Ferreira et al., 1998; Fleischer et al., 1996; Hikita et al., 1976; Iso et al., 2013;

Kothandaraman et al., 2009; Kumar et al., 2014; Li et al., 2014; Lin et al., 2003; Lin and Kuo, 2016; Merchuk, 1980; Nair and Selvi, 2014; Niu et al., 2009; Tavan and Hossein, 2017; Turunen and Haario, 1995; Wang et al., 2013; Weiland et al., 1993). The latter method can be performed either physically or chemically. Physical absorption of CO₂ in water depends on its solubility, which is often the limiting factor to its economic viability from a CO₂ sequestration point of view. However, chemical absorption overcomes this limitation by the action of a chemical reaction taking place between CO₂ and a chemical solvent, thus, enhancing the mass transfer in the liquid phase and the absorption rate for processes that have low CO₂ partial pressure (Aroonwilas et al., 1999; Gavini, 2017; Spigarelli, 2013; Yang et al., 2008, 2011). The chemical reaction is most prominently an acid-base neutralization reaction (Olajire, 2010; Shekhawat et al., 2003) where CO₂ behaves as an acid gas in the presence of a basic solution (Chiang et al., 2017; Kumar et al., 2014; Olajire, 2010; Shen and Yang, 2016; Thiruvalluvan Sujatha et al., 2017).

Various solvents are used in the chemisorption process. These include amine solutions (mono-ethanol amine, MEA, diethanol amine, DEA, and others), carbonate solutions (potassium carbonate, K₂CO₃), alkaline solutions (e.g. aqueous NaOH) and ionic solutions (e.g. ammonia). CO₂ absorption using amine-based solvent is very common in the chemical and oil industry with MEA, DEA and MDEA (methyldiethanolamine) being of primary interest. In fact, MEA is an extensively studied and commercially used method (Chen et al., 2015; Devries, 2014; Samanta et al., 2012; Yang et al., 2008). This process however requires large equipment size, extensive heat input to regenerate MEA, and results in high equipment corrosion rate and solvent degradation (Chen et al., 2015; Devries, 2014; Samanta et al., 2012; Yang et al., 2008). In addition, the high volatility of MEA adds to the operating cost of the process by requiring the continuous addition of make-up streams. Therefore, new and improved solvents with higher CO₂ absorption capacity, faster absorption rate and higher degradation resistances are needed

to reduce equipment size and operating costs. This has been attempted by blending different amine solvents or switching to other solvents that have higher absorption capacity compared to amine-based solvents (Aroonwilas, 2001; Chen and Liao, 2014; MacDowell et al., 2010; Mandal et al., 2001; Saeed et al., 2018). For example, blending MEA and methyl diethanolamine (MDEA) in different ratios has proved to reduce the heating duty for solvent regeneration, given that the chemical stability of the solvent can be maintained (Aroonwilas et al., 1999; MacDowell et al., 2010; Olajire, 2010). However, MDEA still corrodes when exposed to oxygen and provides a lower absorption rate compared to MEA (Isa et al., 2018; Mandal et al., 2001). Alternatively, CO₂ can also be captured using aqueous NaOH solution which actually has a higher CO₂ absorption capacity than MEA (Aroonwilas, 2001; Gavini, 2017; Spigarelli, 2013; Yoo et al., 2013). The theoretical amount of MEA and NaOH to capture a ton of CO₂ is 1.39 and 0.9 tons, respectively. In addition to that, NaOH solution is cheaper than MEA (Yoo et al., 2013). However, NaOH cannot be easily and readily regenerated compared to MEA, which has affected its wide spread usage for this purpose.

Regardless of which solvent is used, CO₂ chemisorption is a multiphase reaction that has been conducted in a multitude of gas-liquid reactors/contactors. These contactors include mechanically agitated vessels (Oyevaar et al., 1988; Oyevaar and Westerterp, 1989), bubble columns (Chen et al., 2014, 2008; Mandal et al., 2008; Vázquez et al., 2000), packed-bed absorption columns (Devries, 2014; Koronaki et al., 2017; Li et al., 2014; Nair and Selvi, 2014; Wang et al., 2013), stirred vessels (Cents et al., 2005) and rotating packed beds (Chiang et al., 2017; Lin et al., 2003; Lin and Kuo, 2016; Luo et al., 2012a; Rajan et al., 2011; Tsai and Chen, 2015; Yang et al., 2011). The design of such units remains very difficult without the use of empirical knowledge and experience and extensive pilot-scale testing. This is mainly caused by the very complex hydrodynamic conditions prevalent in these contactors/reactors with the local value of the mixing intensity, gas holdup, and bubble size distribution depicting large

spatial variations (Andersson et al., 2004; Azizi and Al Taweel, 2015). The chemical absorption of CO₂ using aqueous NaOH has been extensively conducted over the years (Aroonwilas et al., 1999; Chen and Liao, 2014; Chiang et al., 2017; Niu et al., 2009; Tavan and Hossein, 2017; Tsai and Chen, 2015). Most of these studies focused on finding the volumetric mass transfer coefficient, interfacial area, absorption rate and evaluating the performance of the scrubber and packing material, as opposed to investigating CO₂ absorption from an emission reduction point of view. For instance, bubble columns were used to study the influence of CO₂ flow rate at various pH values on the absorption rate. Results show that as the CO₂ flow rate increases and the NaOH concentration increases, the absorption rate increases until it reaches a steady state value (Chen et al., 2008). Additionally, Aroonwilas et al. (1999) studied the CO₂ chemisorption process in a packed bed reactor and focused on investigating the packing performance. They found that structured packing offered superior performance when compared to random packings whereby values of K_{Ga} were as high as 1.5 kmol/m³·h·kPa, owing that to the high CO₂ absorption reaction rate constant (Aroonwilas et al., 1999). In a study by Tsai et al. (2008), CO₂ absorption into NaOH was employed the effective packing area of different packing elements. Tsai and Chen (2015) examined the mass transfer characteristics of a rotating packed bed (RPB) with baffles primarily by quantifying both the liquid side mass transfer coefficient and the effective gas-liquid interfacial area. The latter was determined by employing the chemisorption of CO₂ into NaOH. Results show that the rotating packed bed with static baffles increased the interfacial area by 16-34%. On the other hand, much studies on CO₂ absorption have been carried out to mitigate emissions by evaluating the efficacy of the contactor to carry out the operation. For example, several studies spray dryers (Niu et al., 2009; Tavan and Hossein, 2017) focused on the effect of CO₂ concentration, CO₂ flow rate, NaOH concentration and NaOH flow on the removal efficiency and found that in order to achieve a higher CO₂ removal efficiency, the equivalence ratio of NaOH to CO₂ flow rate should be larger than 4.43.

Values of mass transfer coefficient reported in a rotating packed bed with split packing were two orders of magnitude higher than those reported in a conventional packed column, and this is due to the replacement of the gravity force in packed columns with a centrifugal force in rotating packed beds (Tsai and Chen, 2015). For instance, Lin and Chen (2011) investigated the feasibility of using a cross flow rotating to absorb CO₂ from a gaseous stream into NaOH under various operating conditions including liquid flow rate, gas flow rate and NaOH concentration. However, these studies were conducted without taking into account energy requirements such as that associated with rotation speed. Therefore, continuous efforts in improving the both absorption efficiency and volumetric mass transfer coefficient whilst monitoring the energy consumption of carbon capture into aqueous NaOH solution is sought. One means by which multiphase operations can be drastically enhanced relies on the use of process intensification principles.

Process Intensification is a design methodology whereby cleaner, smaller, safer and more efficient process technologies can be achieved (Reay et al., 2008). It is becoming more popular due to its ability to improve efficiency and process safety while reducing capital and operating cost in various fields related to the chemical process industry such as reactor design (Budzyński et al., 2017; Pangarkar, 2017). In multiphase contactors, mass transfer is typically the rate limiting step (Laakkonen et al., 2006). Generally, the operation of these reactors depends mainly on the efficient dispersion of the phases, thereby, increasing the interfacial area of contact between them and consequently the volumetric mass transfer coefficient. One way of achieving this is by employing tubular reactors equipped with static mixing elements. Such reactors are gaining attention as they provide inherent advantages over conventional reactors, whereby enhanced mixing can be achieved at lower capital and operating costs while handling high flow rates and achieving high mass transfer rates. These reactors have, thus far, been

employed in diverse industries such as the petrochemical and mineral, pulp, paper, paint and pharmaceutical industry, to name a few (Ghanem et al., 2014; Thakur et al., 2003).

Various classifications of these static mixers are available in the literature. Gavrilesco and Tudose (1995), Thakur et al. (2003), Ghanem et al. (2014) and most of them classify these mixers either based on their designs, (e.g. made of helical elements, blades or corrugated sheets) or based on the fluids they are used for (e.g. Newtonian, non-Newtonian, multiphase, etc...) (Gavrilesco and Tudose, 1995). One variant of these mixers, the screen-type static mixers are used to repetitively superimpose an adjustable, radially uniform, highly turbulent field on the nearly plug flow conditions encountered in high-velocity pipe flow. Al Taweel (1996) achieved a 20-fold increase in the interfacial area of contact for a liquid-liquid dispersion compared to Rushton-type impeller, and a 3-fold increase in interfacial area compared to commercially available static mixers, given the same energy input (Altaweel, 1996). Typically, high turbulence and micromixing are generated downstream of a screen-type static mixer (Bourne and Lips, 1991). This leads to the creation of fine drops (or bubble in the case of gas-liquid contacting), and consequently narrow drop size distributions with mean diameters in the order of 40 μm (Azizi and Taweel, 2011; El-Ali, 2001). The combined effect of elevated micromixing intensity and the fine dispersion of drops resulted in high volumetric mass transfer coefficients of 9 s⁻¹ (Al Taweel et al., 2007), in the case of immiscible liquids, and 4.08 s⁻¹ in the case of gas-liquid deoxygenation experiments (Azizi and Al Taweel, 2015). Therefore, the objective of the current study is to investigate the potential of employing screen-type static mixers to intensify the chemical absorption of CO₂ into aqueous NaOH solutions under different operating conditions and design configurations.

CHAPTER II

LITERATURE REVIEW

The reduction of total CO₂ emission into the atmosphere can be mainly done in three ways (Olajire, 2010; Yoo et al., 2013). The first and the second method involve efficient use of energy and switching to other forms of energy such as hydrogen and renewable energy (Olajire, 2010; Yoo et al., 2013), respectively. On the other hand, the third method involves developing technologies to capture and sequester CO₂ (CCS). At the current state of development, switching to non-fossil fuel energy alternatives cannot meet the energy demand and might actually disrupt the existing energy infrastructure (Olajire, 2010). Therefore, mitigating CO₂ through enhancing existing technologies or developing new technologies for carbon capture and sequestration remains an important task. The state-of-the-art process uses aqueous MEA to capture CO₂, however the high cost associated with CO₂ capture and compression limits its implementation (Gabrielsen et al., 2007; Samanta et al., 2012). Therefore, much research has been dedicated towards improving and developing more efficient and cost effective technologies to separate and capture CO₂ (Olajire, 2010; Samanta et al., 2012; Yang et al., 2008).

This section primarily discusses the previous investigations on the chemical absorption of CO₂ in aqueous solutions.

A. Chemical absorption using amine-based systems and carbonate-based systems

Chemical absorption is considered the most effective way of capturing and sequestering CO₂ from a mixture of flue gas having low CO₂ partial pressure (Olajire, 2010; Yoo et al., 2013). Ideally, chemical solvents should have fast CO₂ absorption rate, low regeneration

energy requirement, low degradation rate, low cost and corrosivity (Aroonwilas et al., 1999; Devries, 2014; Gabrielsen et al., 2007; Kim and Cho, 2011; Koronaki et al., 2017). Amine-based absorbents can be basically classified into four groups: primary, secondary, tertiary and sterically hindered amines. Primary and secondary amines share the same reaction mechanism whereby the amine reacts rapidly with CO₂ to form carbamate. As previously mentioned, MEA is a widely used solvent due to its low cost, high reactivity and absorption rate. In fact, MEA has received significant attention as an absorbent for carbon capture, and this is shown through the massive numbers of studies found in the open literature (Aroonwilas et al., 1999; Devries, 2014; Gabrielsen et al., 2007; Kim and Cho, 2011; Koronaki et al., 2017; Kothandaraman et al., 2009; Kumar et al., 2014; Lin and Kuo, 2016; Spigarelli, 2013). Koronaki et al. (2017) developed and validated a rate-based model for CO₂ absorption into MEA that predicts the profile of various process parameters such as temperature and mole fraction as a function of length of the absorber. They recognized the importance of the reaction between CO₂ as a means of reducing the size of the absorber. (Koronaki et al., 2017). Other studies focused on determining the effect of various parameters (pH, mole fraction of CO₂ in the gas mixture, gas flow rate and liquid flow rate) to obtain the optimum conditions for CO₂ capture using MEA in different reactors including, bubble-column scrubber and packed beds (Chen et al., 2014; Kothandaraman et al., 2009; Rezazadeh et al., 2017; Thee et al., 2012). For instance, Chen et al. (2014) found that pH and mole fraction of CO₂ greatly affect the absorption rate in bubble columns whereby low CO₂ concentration in the gaseous phase and high pH favor the absorption rate. Lin et al. (2015) found that the volumetric mass transfer coefficient increases as the gas flow rate and liquid flow rate increased. However, the problem with MEA is that it degrades, requires a lot of energy for regeneration and corrodes the equipment (Isa et al., 2018; Kim et al., 2013; Saeed et al., 2018). Simulations on CO₂ absorption using MEA indicate that there isn't much scope for energy recuperation within the system (Kothandaraman et al., 2009). On

the other hand, DEA, a secondary amine, is less corrosive than MEA and more stable than primary amines, but has a slower reaction rate (Isa et al., 2018; MacDowell et al., 2010).

Tertiary amines possess no hydrogen atom attached to the nitrogen atom, so the carbamation reaction does not take place. Instead, a base-catalysed hydrolysis reaction takes place yielding bicarbonate, HCO_3^- . The heat of the reaction is less than that of the carbamate formation reaction, consequently, reducing solvent regeneration cost (Kim et al., 2013). MDEA, a tertiary amine and a hybrid of MEA and DEA, has a higher degradation resistance and improved CO_2 loading capacity, however it corrodes when exposed to oxygen (Isa et al., 2018; Mandal et al., 2001). Mixed amines have been used as chemical absorbents due to their ability to enhance the previously mentioned desirable qualities of individual amines (Yang et al., 2008). For instance, Idem et al. (2006) analysed the performance of 5M of MEA with a blend of MEA/MDEA having a molar ratio of 4:1. The heating duty for solvent regeneration was greatly reduced upon the addition of MDEA. Chen and Liao (2014) investigated using the blend DEEA (N,N-diethylethanolamine)/EEA (ethylethanolamine) as a chemical solvent to capture CO_2 and found that the mixed solvent proved to have an efficiency in the range 29-98.66% and a mass transfer rate in the range $0.0728\text{-}0.08395\text{ s}^{-1}$ depending on the operating conditions. (Chen and Liao, 2014). The use of sterically hindered amines (such as 2-amino-2-methyl-1-propanol) as CO_2 absorbents has also been reported in the literature. Due to its molecular structure, the carbamate formed is of low stability, therefore, it most likely reacts with water to form free amines or bicarbonate. This helps in reducing the regeneration temperature, but still makes the reaction slower (Kim et al., 2013; Olajire, 2010; Vaidya and Kenig, 2007).

Other investigators focused on the enhancement of CO_2 absorption in carbonate and alkaline systems. Potassium carbonate (K_2CO_3) has been investigated as a solvent for carbon capture due to its low cost, low enthalpy requirements, low toxicity and high degradation

resistance. The only disadvantage is its poor kinetics which in turn require large absorption columns (Isa et al., 2018). Thee et al. (2012) found that utilizing K_2CO_3 reduces energy consumption by 37% in the regeneration process. To overcome its poor kinetics, Hu et al. 2016 and Hu et al. 2017 discussed the potential of using various promoters which could be inorganic (arsenite (Phan et al., 2015; Shen et al., 2013)), organic (MEA (Thee et al., 2012)) or enzymatic based (carbonic anhydrase (Thee et al., 2015)). This in turn improves the reaction kinetics and saves up from the regeneration energy (Hu et al., 2016). Bhosale et al. (2016) investigated the use of ethylaminoethanol, EAE, an organic solvent and promoter for K_2CO_3 solvent (Bhosale et al., 2016). Results show that the absorption rate increased by 35%. However, this investigation is only done on small scale and much more research is needed on pilot scale plants (Bhosale et al., 2016).

B. Chemical absorption of CO₂ into NaOH in different reactors

Alternatively, many investigations have been conducted on the capture of CO₂ using aqueous NaOH solution (Chen et al., 2014; Chiang et al., 2017; Fleischer et al., 1996; Guo et al., 2011; Kordylewski et al., 2013; Lin et al., 2003; Luo et al., 2012b; Niu et al., 2009; Tavan and Hossein, 2017). The reaction of CO₂ with alkaline solvents (such as aqueous NaOH) is considered less complex and simpler than the reaction of CO₂ with alkanol amines as the latter involves the formation of carbamate and bicarbonate (Couchaux et al., 2014; Krauß and Rzehak, 2017; Vaidya and Kenig, 2007; Versteeg et al., 1996). Additionally, NaOH has a strong reactivity with CO₂ and lower vapor pressure (Isa et al., 2018). Several studies by Yoo et al. (2013), Aroonwilas (2001), Devries (2014) and Gavini (2017) showed that NaOH has a higher absorption capacity than MEA. However, according to Isa et al. (2018), using NaOH as an absorbent to capture CO₂ is a costly technology. In addition to that, compared to MEA, the

regeneration of NaOH is not easily achieved due to the formation of Na_2CO_3 , a thermally stable compound, which decomposes into Na_2O . Na_2O , then, decomposes to form NaOH at very high temperatures (Yoo et al., 2013).

Several reactors were used to study the absorption of CO_2 into aqueous NaOH solutions, namely, bubble columns (Chen and Liao, 2014), packed columns (Aroonwilas, 2001; Aroonwilas et al., 1999; Gavini, 2017), rotating packed bed, RPB, (Chiang et al., 2017; Lin et al., 2003; Lin and Kuo, 2016; Tsai and Chen, 2015) and spray dryers (Guo et al., 2011; Niu et al., 2009; Tavan and Hossein, 2017). Studies conducted on CO_2 absorption into aqueous NaOH were mainly carried out for two purposes. The first is involved with determining mass transfer characteristic of gas/liquid reactors (mass transfer coefficient and gas liquid interfacial area) or the influence of various packing material. For instance, the chemisorption of CO_2 into NaOH was used as a test reaction in a bubble column to develop a model for the bubble size distribution and reaction progress (Fleischer et al., 1996). Aroonwilas et al. (1999) studied the influence of different packing elements in a packed bed by on the overall volumetric mass transfer coefficients and found that structured packing offered superior performance when compared to random packings. Many studies used the chemisorption of CO_2 into NaOH to determine the effective gas-liquid interfacial area (Duss et al., 2001; Skoczylas and Majewski, 1991; Tsai and Chen, 2015; Vázquez et al., 2000; Weiland et al., 1993; Yoshida and Miura, 1963). These studies aimed at determining the interfacial area as a function of different parameters such as packing elements, surface tension, liquid flow rate and gas flow rate. In fact, in a recent study conducted by Luo et al. (2017), the use of stainless steel wire mesh packings in a rotating packed bed enhanced the interfacial area and thus more CO_2 was absorbed in NaOH solution-based solvent

On the other hand, other studies on the chemisorption of CO_2 into aqueous NaOH solution were carried to mitigate CO_2 emissions with respect to global warming and climate change.

For instance, bubble columns were used for CO₂ absorption into aqueous NaOH solution, and results show that the removal efficiency and K_{Ga} varied between 30-98% and 0.018-0.058 s⁻¹ respectively (Chen et al., 2014). Numerical simulations were also done on the chemisorption of CO₂ into NaOH solution in a bubble column equipped with screen meshes. It was found that the insertion of multiple screens can greatly improve the reactor performance of a bubble column by decreasing the Sauter mean diameter of the bubble, thereby increasing the interfacial area of contact between the phases and enhancing the mass transfer and chemical reaction rate (Jain et al., 2015). A great number of studies have been conducted on packed beds with different packing types in order to determine the effect of various operating and design conditions on the mass-transfer coefficient. Gavini (2018) studied the absorption of CO₂ into NaOH in a randomly packed column and found that the overall gas mass transfer coefficient increased from 37.2 mol.m⁻³.min⁻¹ to 45.67 mol.m⁻³.min⁻¹ upon increasing the NaOH concentration from 0.003 M to 0.01 M due to the rapid reaction occurring. These results were comparable to industry standard K_{Ga} data which is in the range of 25-75 mol.m⁻³.min⁻¹ (Gavini, 2017). Aroonwilas (2001) explored the effect of various operating conditions (such as gas and liquid flow rates and temperature of the absorbent) and design conditions on the CO₂ absorption efficiency. The absorption performance did not get affected by the change in gas load, however it increases with the increase in liquid load. Moreover, as the temperature of the liquid phase increases, the mass transfer efficiency increases until it reached a particular temperature where the mass transfer efficiency starts decreasing. It was also observed that Mellapak 500Y exhibited superior mass transfer coefficients compared to the other structured packings which is basically attributed to its low corrugation angle that enhances the wetted packing surface (Aroonwilas, 2001). In another study by Aroonwilas et al. (1999), structured packing have proved to offer superior performance compared to random packings whereby values of K_{Ga} were as high as 1.5 kmol.m⁻³.h⁻¹.kPa⁻¹. It was also proven that the higher the concentration of

NaOH, the higher the absorption efficiency (Aroonwilas et al., 1999). Although these studies are conducted on the industrial scale, the energy requirement, a very important parameter that influences the economic feasibility of a process, was not directly determined.

Mass transfer coefficients and mixing efficiency can be significantly increased by using rotating packed beds (RPB), and this is due to the replacement of the gravity force in packed columns with a centrifugal force in rotating packed beds (Tsai and Chen, 2015). Consequently, a reduction in size and capital of a RPB was realized and instigated great effort in the field of process intensification (Tsai and Chen, 2015). Lin and Kuo (2016) investigated the CO₂ absorption in a RPB having two different design packing: blade and structured packing, and found that for the same conditions the blade packing generated a higher CO₂ absorption rate than structured packings. In addition to that, it was found that the higher the gas and liquid flow rate, the higher the volumetric mass transfer coefficient (Lin and Kuo, 2016). Lin et al. (2003) investigated CO₂ absorption into NaOH in a cross-flow rotating packed bed and found that K_{Ga} values increased with liquid flow rate and NaOH concentration. In addition to that, K_{Ga} values in a cross-flow RPB reached 1.4 s⁻¹ and were higher than that in a countercurrent-flow RPB for 10% v CO₂ concentration and 1 M NaOH (Lin et al., 2003). Recent enhancement on the CO₂ absorption efficiency to more than 90% was realized upon the addition of glycerol to the aqueous NaOH solution in a rotating packed bed (Chiang et al., 2017). The centrifugal force, resulting from the addition of glycerol, actually intensified the mass transfer of CO₂ and the resulting heating capacity of the aqueous NaOH solution was lowered leading to a lower heating requirement for solvent regeneration (Chiang et al., 2017).

Other studies on spray dryers (Niu et al., 2009; Tavan and Hossein, 2017) focused on the effect of CO₂ concentration, CO₂ flow rate, NaOH concentration and NaOH flow on the removal efficiency and found that in order to achieve a higher CO₂ removal efficiency, the equivalence ratio of NaOH to CO₂ flow rate should be larger than 4.43. Similarly, Guo et al.

(2011) investigated the effect of different operating conditions such as concentration of aqueous NaOH solution and total gas flow rate on removal efficiency. Results show that, the higher the NaOH concentration and the lower the gas mixture flow rate, the higher the CO₂ removal efficiency (Guo et al., 2011). Although studies conducted on rotating packed beds touch on the principles of process intensification, the conditions at which the experiments are conducted do not reflect the industrial scale conditions. In addition to that, the energy requirement for the chemisorption process was not assessed as a factor that affects the feasibility of the process.

Therefore, this raises the need to develop cheaper and more efficient carbon capture technologies whilst evaluating the volumetric mass transfer coefficient, removal efficiency and energy requirement.

CHAPTER III

EXPERIMENTAL SECTION

A plug flow reactor/contacter equipped with screen-type static mixers was employed to determine the absorption of CO₂ into aqueous NaOH solutions. In this section, the chemisorption reaction is described, followed by a description of the experimental setup used and the range of parameters investigated. Finally, the method of analysis by which the volumetric mass transfer coefficient, efficiency and power consumption in continuously flowing reactors can be calculated is presented.

A. Reaction of CO₂ with aqueous NaOH

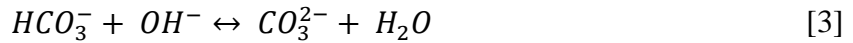
The mechanism of CO₂ absorption in an NaOH aqueous solution is well established (Fleischer et al., 1996; Hikita et al., 1976; Krauß and Rzehak, 2017; Niu et al., 2009; Wang et al., 2010) and can be explained as follows:

Firstly, gaseous CO₂ is physically absorbed into aqueous CO₂.



The reaction of CO₂ with water is only relevant at low pH and can be ignored at high pH (Fleischer et al., 1996). Therefore, the aqueous CO₂, then, gets chemically absorbed by hydroxide ions, OH⁻, to form bicarbonate, HCO₃⁻ and carbonate CO₃²⁻ according to the following reactions:

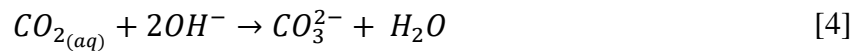




Reaction [3] is a second order reaction or, in some instances, it can be considered as a pseudo-first order reaction (Yoo et al., 2013)

Both reactions [2] and [3] are reversible and exothermic, with reaction [3] being the fastest and having the higher reaction rate as it is a proton transfer reaction (Hikita et al., 1976). Hence, reaction [2] is the rate limiting step (Pohorecki and Moniuk, 1988). The reaction rate therefore depends on the rate of reaction [2], which is, in turn, highly dependent on the ionic strength of the solution.

In strong alkaline solutions, the equilibrium concentration of HCO_3^- is neglected, which is the case in the current investigation (Hikita et al., 1976), and therefore, the overall reaction can be reduced to:



B. Experimental Setup

In this study, a tubular plug flow reactor equipped with screen-type static mixers was used to quantify the volumetric mass transfer coefficient, power consumption, and efficiency under different hydrodynamic conditions. The continuous flow experimental setup is shown in the schematic represented in Figure 1. Reverse osmosis (RO) water was stored in a 500L polyethylene tank from which it was pumped into the gas-liquid contactor system using a single stage centrifugal pump (Pedrollo[®], model AL-RED 135m). A high concentration stock NaOH solution was prepared by dissolving NaOH pellets of purity >99.15% (Formosa Plastics) in reverse osmosis water and stored in a separate 250 L tank from which it was pumped using a dosing pump (Prominent, model CONCEPT PLUS/PVT, Teflon) into the water entering the

reactor/contacter. The dosing was conducted to increase the pH of the aqueous phase to a value of 12.6 ± 0.2 . This value of pH was then maintained constant throughout all experiments, regardless of the flow rates. The overall liquid phase flow rate (aqueous NaOH) was then measured using a paddle flow meter (Omega engineering, FP-90 Series) and typically varied from 20.6 to 53 L/min, which corresponds to liquid phase superficial velocities, U_L , ranging from 0.7 to 1.8 m/s and a pipe Reynolds number (based on total velocity) ranging from 24,830.94 to 50,000. To simulate the flue gas emitted in the industries, a 30%v/v CO₂/air gas stream was used throughout the experiments. Such conditions of high CO₂ concentrations are common in the cement and steel industries (Yoo et al., 2013). The pure CO₂ stream was always mixed with the exact amount of air (both flow rates were controlled using Omega Engineering, FMA-series mass flow controllers) before it was sent to the reactor/contacter where it enters it co-currently with the caustic aqueous phase. The total gas flow rate ranged from 2.9 L/min to 17.66 L/min in order to attain gas volume fractions of 10, 20 and 30%.

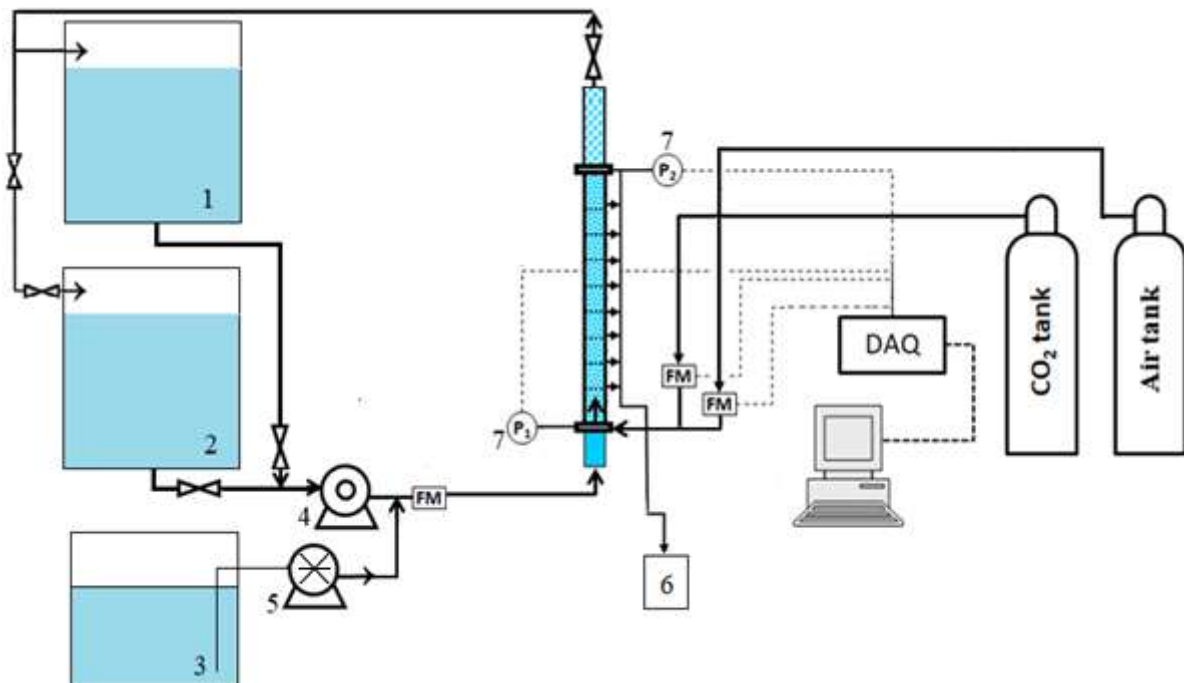


Figure 1: Schematic Representation of the experimental setup (1): supply tank (2): drain tank (3):NaOH tank (4):centrifugal pump (5): dosing pump (6): samples extracted for analysis (7): pressure sensors

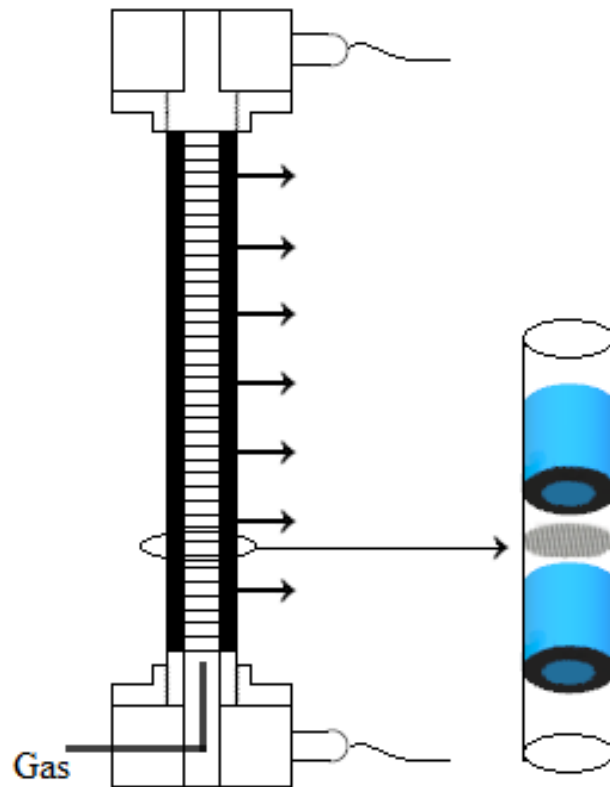


Figure 2: Reactor Internals

Gas-liquid contacting took place in a 900 mm vertical pipe. Its vertical orientation ensures that all multiphase radial nonuniformities and temporal flow nonuniformities due to the action of gravity, are eliminated. In the mixing section, commercially available stainless steel (type 304) woven meshes (Ferrier Wire, Toronto, Canada) were inserted to act as static mixers. The characteristics of the screens are given in Table 1, and were inserted at 40 mm spacing in order to better disperse the gas-liquid flow (Al Taweel et al., 2007, 2005; Munter, 2010; Turunen and Haario, 1995) and intensify the mass-transfer-limited reaction (Al Taweel

et al., 2013). To ensure that the screens are held apart and remain perpendicular while the fluid flows inside the reactor, Plexiglas cylindrical spacers of 20 mm length and 25 mm ID were used and were tightly inserted in a clear PVC pipe (48 mm OD and 40.9 mm ID) , as can be seen in Figure 2. Such configuration insured that spacers remained immobile while providing the effective flow diameter of 25 mm.

The plain weave wire gauzes that were used are typically characterized by their mesh number, Mn , which represents the number of openings in one inch, the wire diameter, b , and the mesh size, M , which corresponds to the center-to-center distance between two adjacent wires. Accordingly, the open area of the screen can be deduced from the mesh size, M , and wire size, b , according to Equation (5). Figure 3 shows a sketch of a screen element and highlights its various geometric/design parameters.

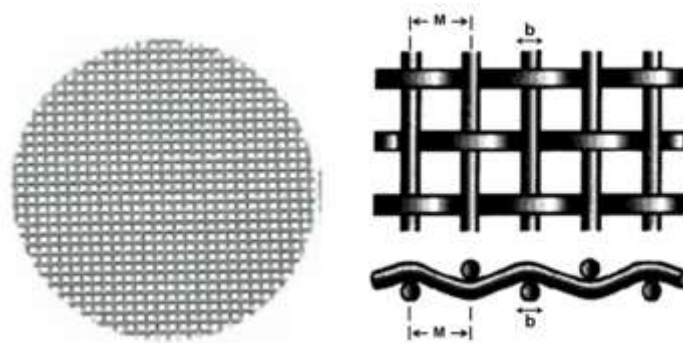


Figure 3: Screen-type static mixer

$$\alpha = \left(\frac{M - b}{M} \right)^2 \times 100 \quad [5]$$

Table 1: Characteristics of the investigated stainless-steel plain weave wire meshes

Mesh Number, Mn	Wire Size, b (μm)	Mesh size, M (μm)	Open Area, α (%)
30	304.8	838.2	40.5

50	228.6	508	30.25
80	139.7	317.5	31.36
100	114.3	254	30.25

The setup was provided with seven sampling ports placed 100 mm apart. At each sampling port, the spacer had a 2 mm deep groove around its circumference and four 2-mm holes were drilled at 90° angles for withdrawing liquid samples and ensuring a more representative sample composition.

The pressure at the inlet and the outlet of the mixing section was measured using pressure transducers with a response time less than 0.01 s (Omega Engineering, PX-303 Series). All sensors were controlled using a National Instruments data acquisition board (National Instrument, model NI USB - 6212) and a specially developed LabVIEW program. Although the setup is capable of operating in the recycle mode, all the experiments reported in this investigation were conducted using a once-through approach.

In this study, various operating conditions were varied in order to investigate the potential of employing screen-type static mixers to intensify the chemical absorption of CO₂ into aqueous NaOH solutions. These conditions include varying the total velocity (1, 1.3, 1.6 and 2 m/s), gas holdup (10, 20 and 30%), and the screen-type static mixers geometry mesh number (30, 50, 80 and 100) and are summarized in Table 2.

Table 2: Operating Conditions

Condition	Value
Pipe diameter (mm)	25

Number of screen elements	15
Inter screen spacing (mm)	40
Screen open area (%)	30.25 – 40.5
Liquid superficial velocity (m/s)	0.7 – 1.8
Gas velocity (m/s)	0.1 – 0.6
Total velocity (m/s)	1 – 2
Dispersed phase holdup (%)	10, 20 and 30
Pipe Reynolds number (based on total velocity)	25000 – 50000
Residence time (s)	0.39 – 0.78

C. Method of Analysis

The performance of the reactor was evaluated based on the volumetric mass transfer coefficient, $k_L a$, CO₂ removal efficiency and the energy required to perform the operation.

1. Estimation of the overall volumetric mass transfer coefficient

To calculate the volumetric mass transfer coefficient, the concentration of reacted CO₂ in the liquid phase and the equilibrium concentration of CO₂ are needed. In the current investigation, seven samples were always withdrawn from the reactor at various locations (corresponding to various reaction times) and were used to track the steady-state evolution of the chemisorption process. This method of estimating $k_L a$ is far more superior to that obtained

using only the two-point approach which relies on the inlet and outlet concentrations (Al Taweel et al., 2005; Azizi and Al Taweel, 2015).

Due to the short inter-screen spacing and the high flow velocities, nearly plug flow conditions, characterized with low axial dispersion coefficients prevail inside the reactor/contactor (Abou Hweij and Azizi, 2015; Azizi and Hweij, 2017; Ziókowski and Morawski, 1987). Therefore, the overall volumetric mass transfer coefficient can be described by a first order differential equation, according to Equation (6).

$$\text{Mass transfer rate} = \frac{dC}{dt} = k_L a. (C_{CO_2}^* - C) \quad [6]$$

Integrating equation [6] from $t=0$ to $t=t$ with boundary conditions $(C_{CO_2}^* - C) = (C_{CO_2}^* - C_{CO_2})_0$, which represent the initial conditions at the reactor inlet and $(C_{CO_2}^* - C) = (C_{CO_2}^* - C_{CO_2})_t$, which represent the conditions at time t , and assuming a constant value for $k_L a$, yields the following expression.

$$\ln \left[(C_{CO_2}^* - C_{CO_2})_t \right] = -k_L a. t + \ln \left[(C_{CO_2}^* - C_{CO_2})_0 \right] \quad [7]$$

A linear relationship therefore exists between $\ln(C_{CO_2}^* - C_{CO_2})$ and t with a slope of $-k_L a$. In the chemisorption of CO_2 into aqueous NaOH, neglecting the local gas side mass transfer coefficient depends on the process parameters. In this study, it is important to note that the gas side mass transfer coefficient can be neglected as the fluid flow is turbulent and well-mixed. In addition to that, it was found that when the partial pressure of CO_2 is low and NaOH is found in excess, under similar operating conditions to this work, the local gas side mass transfer coefficient was neglected (Ferreira et al., 1998). Therefore, the CO_2 absorption process is controlled by the liquid film resistance. To determine $k_L a$, C_{CO_2} and $C_{CO_2}^*$ should be determined.

a. Concentration of the reacted CO₂ in the liquid phase

The carbonate content, which corresponds to the CO₂ transformed and reacted from the gaseous phase to the liquid phase, was measured by withdrawing liquid samples from each sampling port and titrating it using duplicate measurements with HCl and using two indicators (phenolphthalein and bromocresol green methyl red), according to Warder and Winkler method. This helps in determining the concentration of hydroxide and carbonate ions and is adapted from Crossno et al. (1996). Titration to the first equivalence point converts all NaOH and CO₃²⁻ found in the sample into bicarbonate, HCO₃⁻, and titration to the second equivalence point converts all HCO₃⁻ into carbonic acid, H₂CO₃ (Crossno et al., 1996). It is important to note that a control sample was taken before gas injection, for each experiment, to test for the carbonate concentration in the aqueous phase before any gas was injected.

b. Concentration of CO₂ in the liquid phase at equilibrium with the gas phase

The equilibrium interface concentration of CO_{2(g)} in the liquid phase is described by Henry's law.

$$CO_{2(aq)} = H \cdot P_{CO_2} \quad [8]$$

Therefore, the concentration of CO₂ in the liquid phase, C_{CO₂}^{*}, at equilibrium with the gas phase, can be determined according to Henry's law and is highly dependent on Henry's constant according to equation [8].

Henry's constant for CO₂ in an aqueous electrolyte solution can be calculated using the following equations (Pohorecki and Moniuk, 1988).

$$\log \frac{H}{H(\text{water})} = - \sum_j I_j \cdot h_j \quad [9]$$

Where, H = henry's constant for CO₂ in an electrolyte solution, kmol.m⁻³.bar⁻¹;

H_{water} = henry's constant for CO₂ in water, kmol.m⁻³.bar⁻¹;

I_j = ionic strength, kmol.m⁻³;

h_j = contribution value for each ion, m³/kmol;

$$\log(H_{\text{water}}) = 9.1144 - 5.9044 * 10^{-2}T + 7.8857 * 10^{-5}T^2 \quad [10]$$

$$h_j = h_+ + h_- + h_g \quad [11]$$

$$I_j = C_j \cdot z_j \quad [12]$$

Where, C_j= concentration of the ion, kmol.m⁻³;

z_j = ion electric charge;

The values of the contributions of each ion, h_j, are represented in the table below(Pohorecki and Moniuk, 1988)

Table 3: Ion contribution values

Ion	Ion Contribution (m ³ /kmol)
Na ⁺	0.091
K ⁺	0.074
CO ₃ ²⁻	0.021
CO ₂	-0.019

OH ⁻	0.066
-----------------	-------

Once Henry's constant is obtained for every sample, the concentration of CO₂ in the liquid phase that is in equilibrium with the gaseous phase is calculated using the experimental pressure value and Henry's constant.

2. Efficiency

CO₂ removal efficiency is used as a direct index of the efficiency of the absorption process. In the case of CO₂ absorption into aqueous NaOH solution, the removal efficiency is reported as

$$E (\%) = \frac{n(CO_3^{2-})_{formed}}{n(CO_2)_{injected}} \times 100 \quad [13]$$

Where, E = absorption efficiency, %

$n(CO_3^{2-})_{formed}$ = molar flow rate of the carbonate formed as a result of the chemical reaction at each sampling point, mol/min;

$n(CO_2)_{injected}$ = molar flow rate of CO₂ injected into the system, mol/min;

CO₂ removal efficiency is not only used to evaluate the overall efficacy of the CO₂ absorption for different operating conditions but is also an important factor when it comes to tracking the efficiency of each experimental condition v/s time.

3. Power Consumption

Power consumption, which primarily depends on pressure drop and the total superficial velocity, is one of the most important design criteria as it determines the economic desirability of the reactor/contactor. The energy input into a gas-liquid contactor can be described in multiple ways. For instance, it could be reported as the amount of energy supplied per unit time, E , or amount of energy supplied per unit time and unit mass, ε as described by the equations below (Azizi and Al Taweel, 2015).

$$E = \Delta P \cdot (Q_G + Q_L) \quad [14]$$

$$\varepsilon = \frac{Q_L \Delta P}{\rho_L V_L} = \frac{U_L \Delta P}{\rho_L L(1 - \phi)} \quad [15]$$

The parameters are considered to characterize the energy requirement in a gas liquid contactor. However, the energy requirement obtained by these parameters could reach high values, however, residence time requirements should be factored in before assessing the actual power consumption. Therefore, in the case of continuously flowing systems, another approach has been suggested which better reflects the energy input as it takes into account the residence time that is required in the contactor (Koglin et al., 1981; Al Taweel and Walker, 1983). It is described as the specific energy consumption term, E_{spm} (J/kg), which is the power needed to process a unit mass of the flowing mixture and can be calculated from the following equation.

$$E_{spm} = \frac{\Delta P \cdot (Q_G + Q_L)}{\rho_{mix} \cdot V} \cdot t_{res} \quad [16]$$

Where, E_{spm} = specific energy consumption, J/kg;

ΔP = pressure difference between the inlet and outlet, Pa;

Q_G = gas flow rate, m³/s;

Q_L = liquid flow rate, m³/s;

V = volume of the reactor, m³;

ρ = density of the mixture, kg/m³;

As can be noticed from the equation above, the pressure drop greatly affects the specific energy consumption, and is as such an important design criterion for a static mixer. In this study, three main factors contribute to the overall pressure drop, namely, pressure drop due to the difference in static head, pressure drop caused by skin friction at the pipe wall and pressure drop caused by the insertion of screen-type static mixers across the reactor. These contributions vary depending on the operating parameters, such as the gas and liquid flow rates, and design parameters such as the length of the reactor (Azizi and Al Taweel, 2015). In this study, the pressure drop due to the screens is expected to be the dominant one due to the turbulent flow conditions encountered in this system.

CHAPTER IV

RESULTS AND DISCUSSION

In this study, the volumetric mass transfer coefficient, efficiency, and the specific energy consumption rate were determined as a function of various operating and design conditions. These values would indicate the enhancement and intensification of interphase mass transfer of CO₂ into aqueous NaOH solution along with the energy requirement for each operating and design condition. It is important to note that the gas-liquid dispersion, under all operating conditions, remained in the bubbly regime.

A. Pressure drop

As previously mentioned, one of the most important parameters that determine the power consumption is pressure drop. In this investigation, values of pressure drop were recorded against total superficial velocity and liquid superficial velocity for four different mesh geometries.

In the case of tubular reactors equipped with static mixers, the total pressure drop is the sum of the pressure drop in the empty pipe and the pressure drop for the flow passing through the screens. Pressure drop across any screen geometry is caused by viscous and inertial resistances, the former being dominant in the laminar flow regime. The latter is dominant at high superficial velocities, which is the case in this study. These pressure losses are basically caused by the turbulent vortices associated to the sudden expansion and contraction caused by the screens inserted across the flow in the reactor (Azizi and Al Taweel, 2015). This causes the pressure drop to increase significantly, regardless of the mesh geometry, compared to the flow in an empty pipe. On another note, pressure drop across a screen is highly influenced by the

geometrical characteristics of static mixer (mesh number, wire size, open area, free area for flow, etc.) (Munter, 2010). The pressure drop is expected to increase with screen-type static mixers having higher number of openings per screen due to the intensity of the generated turbulent vortices. As can be seen in Figure 4a, results show that the highest pressure drop was generated from the screens with Mn = 80 negating what was expected even though the screens with Mn = 80 had an open area slightly larger than that of Mn = 100. This is because the hydrodynamics of the flow through screen- mixers are affect by the wire size and consequently show a larger dependence on the wire Reynolds number, Re_b , rather than the pipe Reynolds number (Abou Hweij and Azizi, 2015). When pressure drop is plotted against wire Reynolds number, screens with Mn = 100 showed the largest pressure drop as expected.

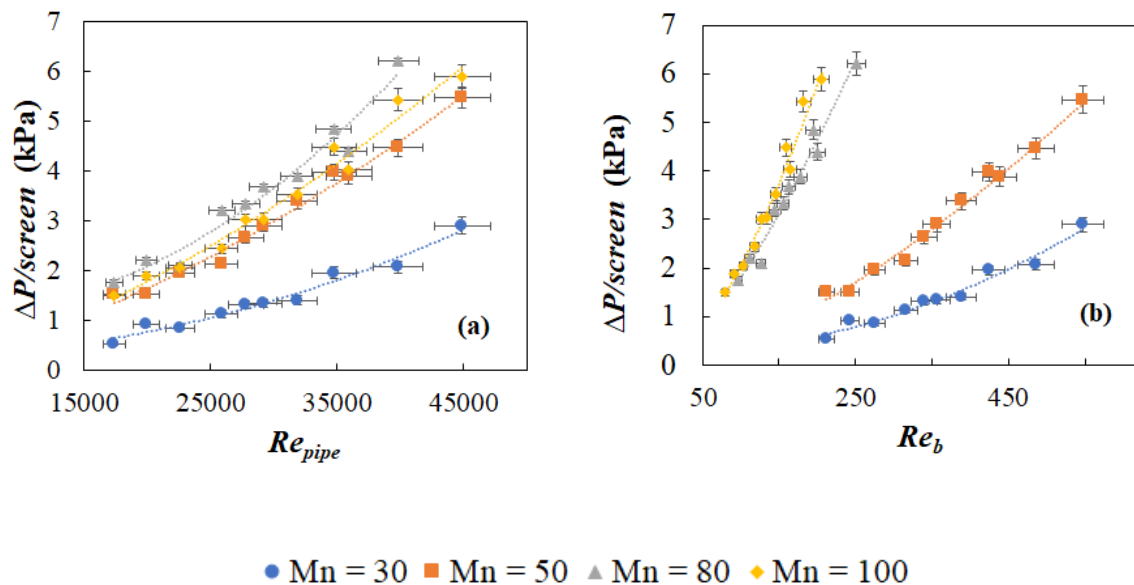


Figure 4: Pressure drop for four different screen geometries versus: (a) Empty pipe Reynolds number, Re_{pipe} and (b) Wire Reynolds number, Re_b for $\Phi = 0\%$

The pressure drop was also recorded for two-phase gas-liquid flows. It was found that, regardless of the mesh geometry, the introduction of a gaseous phase decreased the pressure

drop for a given liquid superficial velocity. This is clearly shown in Figure 5a where it is clear that as the holdup increases, the pressure drop keeps on decreasing for the same total superficial velocity. This can be attributed to two factors, namely, the formation of a lower dispersion density which lowers the kinetic energy of the micro-jets formed by the screen, and the reduction in the drag coefficient of the screen due the formation of fine bubbles in the flow path (Azizi and Al Taweel, 2015). However, as can be seen from Figure 5b, when plotting the pressure drop against the liquid flow velocity, the magnitude did not change regardless of gas holdup. This reveals that the pressure drop is independent of the gas velocity and is in-line with the results obtained by Azizi and Al Taweel (2015).

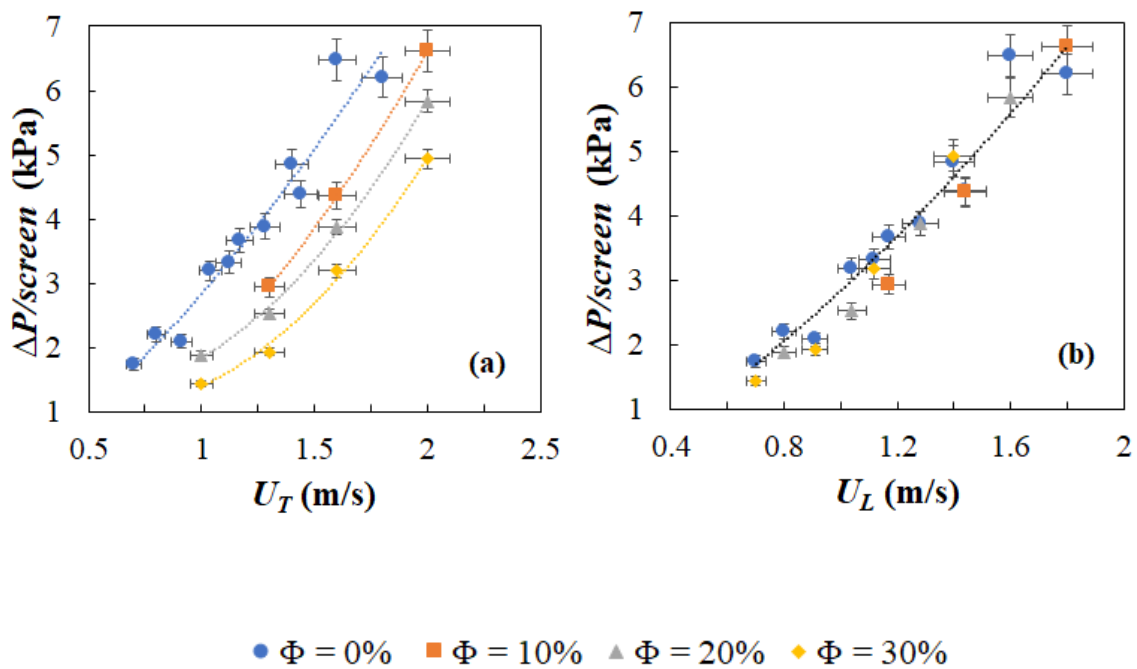


Figure 5: Effect of gas holdup on the pressure per screen: (a) pressure drop versus superficial velocity of gas – liquid mixture and (b) pressure drop versus liquid velocity for $Mn = 80$

B. Volumetric mass transfer coefficient

The volumetric mass transfer coefficient is the most important factor that characterizes mass transfer in multiphase reactors. To calculate k_{LA} , the concentration of CO_2 in the liquid phase at equilibrium with the gas phase, $C_{\text{CO}_2}^*$, and the concentration of CO_2 absorbed into the liquid phase should be determined. The former is obtained from the local pressure and the latter from titrating the liquid phase at various sampling points along the length of the reactor. In this section the effect of varying the operating and design conditions will be presented.

1. Effect of liquid flow rate

The superficial liquid velocity is an important parameter as it controls the residence time in the contactor, intensity of the generated turbulence and the energy dissipation rate (Al Taweel et al., 2005). The higher the velocity, the lower the residence time will be but the higher the turbulence and energy dissipation rate. Therefore, the gaseous bubbles become more dispersed and bubble breakage becomes dominant due to the elevated turbulence downstream of the screen, causing an increase in interfacial area of contact between the phases. This, in turn, causes an increase in k_{LA} , as can be seen in Figure 6 (Al Taweel et al., 2005; Azizi and Al Taweel, 2015). In addition to that, it is expected that the screen with highest mesh number would generate the highest values of k_{LA} as the superficial liquid velocity increases. This is due to the combined effect of the higher number of openings and smaller percentage open area in the screens having the highest mesh number, and the turbulence generated from the high superficial liquid velocity. (Al Taweel et al., 2005). This explains why k_{LA} is the highest for screens with the highest mesh number, i.e. $M_n = 100$. The variation of k_{LA} with total superficial velocity for all four screen geometries are shown in Figure 6. The highest recorded k_{LA} values corresponded to the highest liquid flow rates for any gas holdup with values ranging between 0.1156 and 1.3653 s^{-1} .

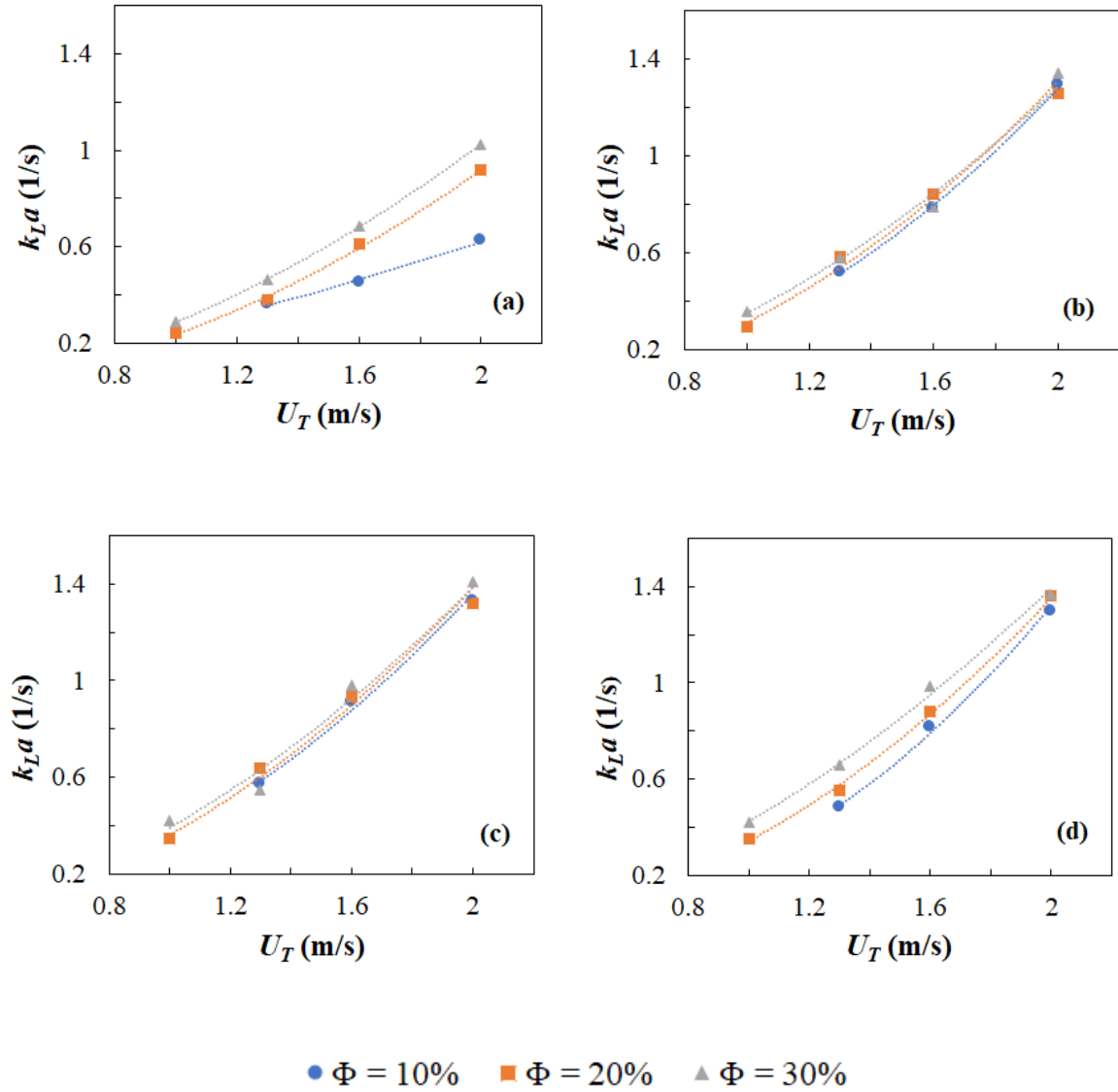


Figure 6: Effect of Superficial velocity and gas holdup on $k_{L}a$:(a) $Mn = 30$, (b) $Mn = 50$, (c) $Mn = 80$ and (d) $Mn = 100$

2. Effect of gas flow rate

The effect of gas holdup, ϕ , was investigated while varying liquid flow rates and screen geometries. As the gas-liquid flow ratio increases, the bubble population density increases and so does the mean bubble diameter due to the increase in bubble collision and coalescence rate. The effect of increasing ϕ on the volumetric mass transfer coefficient depends on the values of

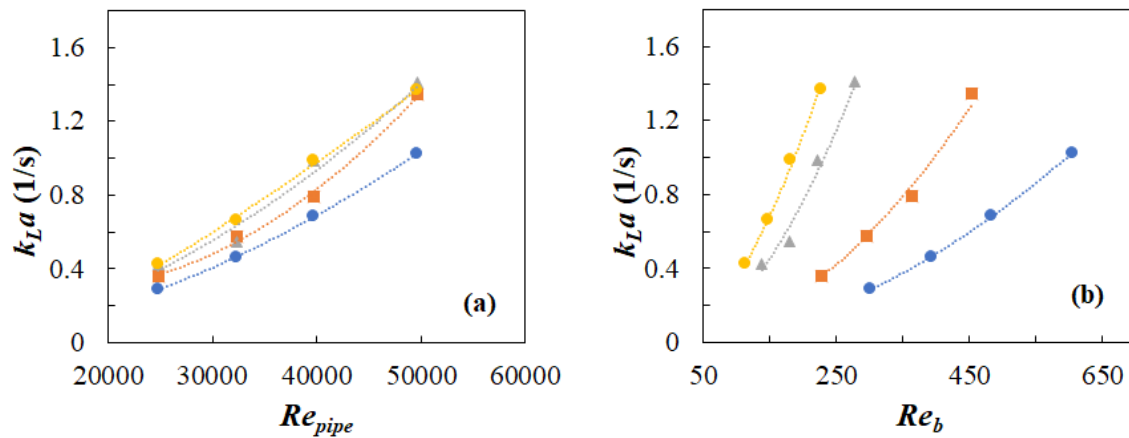
both k_L and a . As can be seen from Figure 6, k_{LA} increases as the gas superficial holdup increases regardless of the mesh geometry.

Thiruvalluvan Sujatha et al. (2017) found that, in a bubble column without internal mixing elements, as the superficial velocity of the gas increases, smaller bubbles are formed as a result of bubble breakup. However, with the presence of internal mixing element, screen-type static mixers, the bubbles produced were even finer for a mesh opening of 3.7 mm (Thiruvalluvan Sujatha et al., 2017). Similarly, in this investigation, the effect of gas holdup for various mesh geometry was observed. It was found that the highest k_{LA} values were achieved at the highest gas holdup ($\phi = 30\%$). This is attributed to the better bubble breakage which is expected with the increase in gas holdup using screen mixers with high mesh number in the turbulently flowing gas-liquid system. These results are in agreement with other studies (Azizi and Al Taweel, 2015; Thiruvalluvan Sujatha et al., 2017).

3. Effect of Reynolds number

The characteristic length in Reynolds number is an important factor when it comes to investigating the turbulence of the flow in reactors equipped with screens as it is an important factor that judges the performance of the static mixer. As explained by Abou Hweij and Azizi (2015), there exists several characteristic lengths (e.g. diameter of the pipe, wire diameter, mesh opening). Therefore, values of k_{LA} were plotted against the various Reynolds number (empty pipe Reynolds number, Re_{pipe} ; wire Reynolds number, Re_b ; mesh Reynolds number, Re_M ; individual-jet Reynolds number, Re_j ; and the macroscopic jet Reynolds number, Re_{jet}) for the different screen geometries used in this investigation, at the same holdup. As can be seen from Figure 7a, k_{LA} increases as the screen mesh number increases. However, the values obtained are relatively close to each other and are hard to distinguish at high gas holdup. Hence,

the effect of screen geometry is better observed when using Reynolds number with other characteristic lengths. As expected, similar trends were obtained for k_{LA} versus Re_b , Re_M and Re_j as can be seen from Figure 7b, c and d due to characterizing the Reynolds number by the mesh size and wires size. Finer bubbles and better dispersion occur when a decrease in mesh size and wire size is realized. Therefore, for all the previously mentioned conditions, the effect of screen geometry becomes much clearer on the values of k_{LA} . Particularly, when k_{LA} is plotted against Re_b , Re_M and Re_j , it can be clearly seen that the smaller the wire size or mesh size, the higher the k_{LA} values. On the other hand, k_{LA} decreases as the screen mesh number increases when utilizing the macroscopic jet Reynolds number, Re_{jer} . In this case, the macroscopic jet Reynolds number, which is the equivalent of the pipe Reynold number divided by the open area, is only distinguished among the different screens based on the open area, which are closely related to each other for the different screen meshes used.



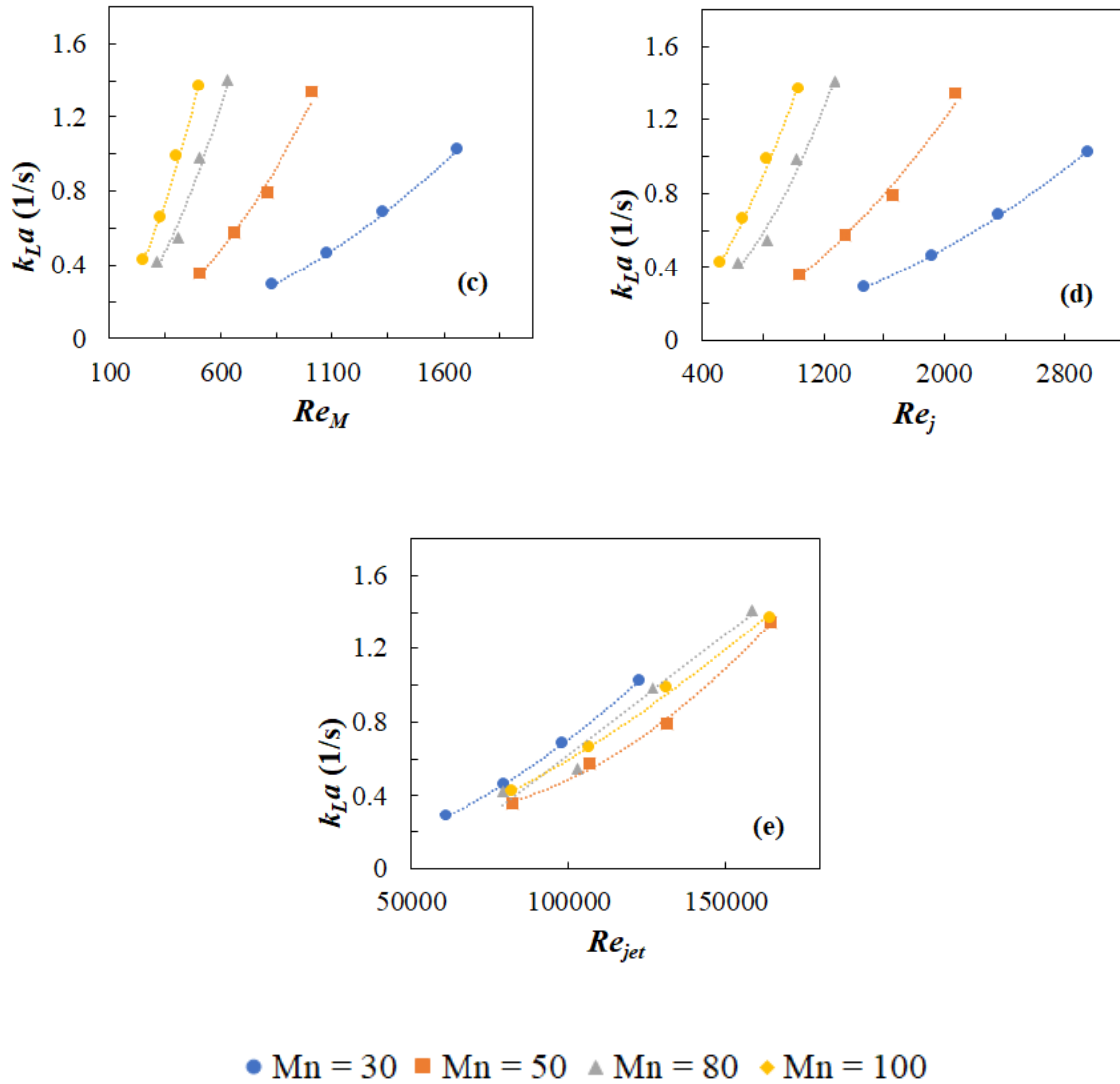


Figure 7: The variation of k_{La} with the various Reynolds numbers for all four screen geometries for $\phi = 30\%$: (a) Re , (b) Re_b , (c) Re_M , (d) Re_j and (e) Re_{jet}

C. CO₂ Removal Efficiency

Another important criterion that tracks the efficiency of the chemisorption operation is the CO₂ removal efficiency. The ability to sample the liquid phase at various locations along the length of the reactor, allows for a better characterization of the removal efficiency and the ability to track its temporal variation.

The effect of liquid flow rate, gas hold-up and mesh geometry on the removal efficiency were investigated. Results show that, for the same experimental conditions, as the screen mesh number increases, the efficiency rapidly increases until a plateau is reached. This phenomenon can be clearly observed in Figure 8. As such, screens with high mesh numbers, will offer the advantage of a further reduction in reactor length with its subsequent consequences on both operating and capital costs.

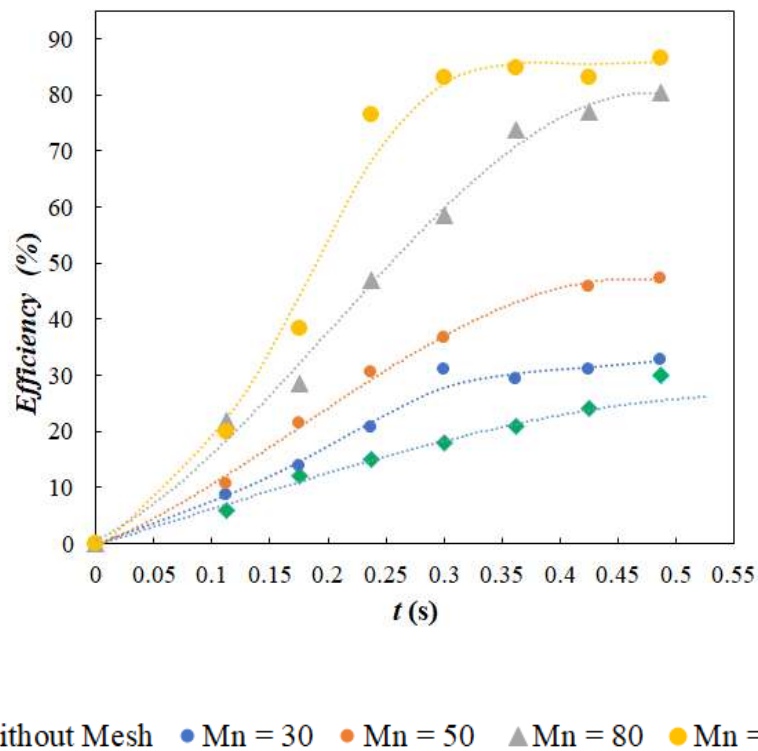
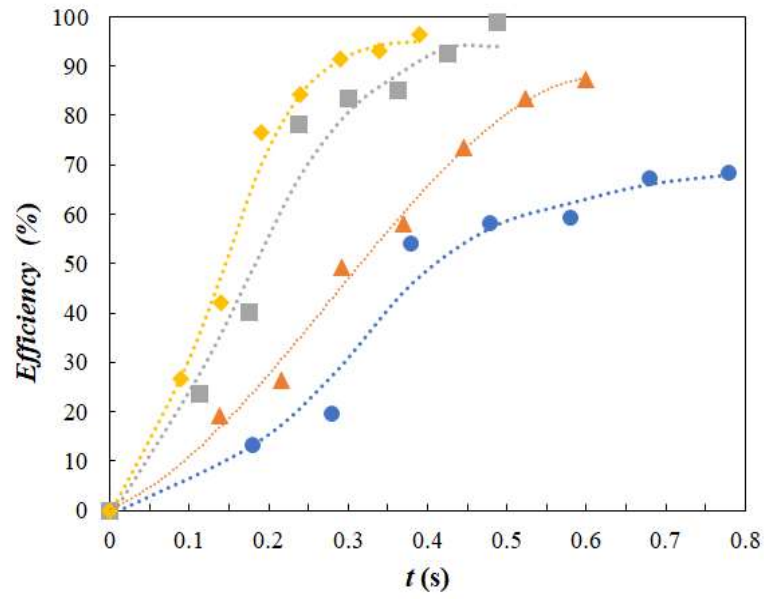


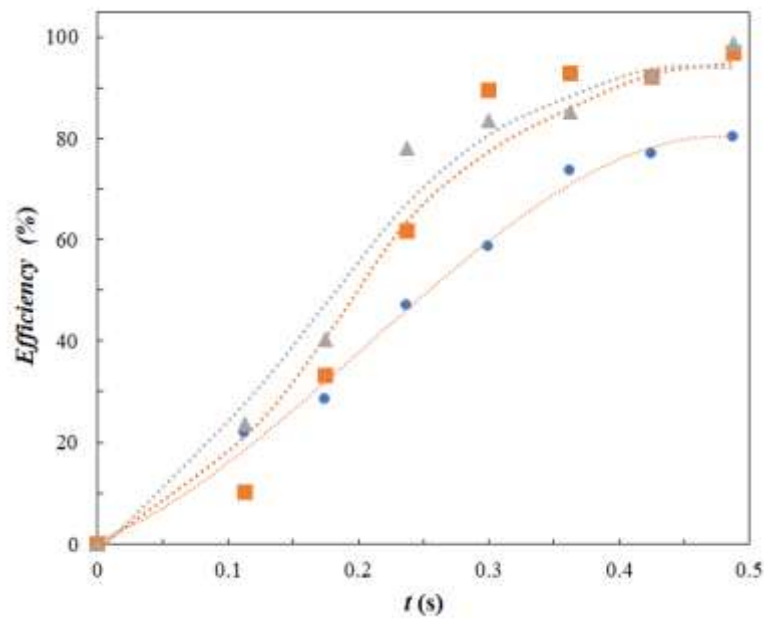
Figure 8: Effect of mesh geometry on efficiency at 1.6 m/s and $\Phi = 10\%$

Similar results were obtained when analysing the effect of gas-hold up and total superficial velocity. For the same holdup and screen geometry, as the total superficial velocity increases, efficiency increases, which is in agreement with Niu et al. (2009) and Guo et al. (2011). On the other hand, for the same total superficial velocity and mesh geometry, as the holdup increases the efficiency increases, which is in alignment with Guo et al. (2011).



● U = 1 m/s ▲ U = 1.3 m/s ■ U = 1.6 m/s ◆ U = 2 m/s

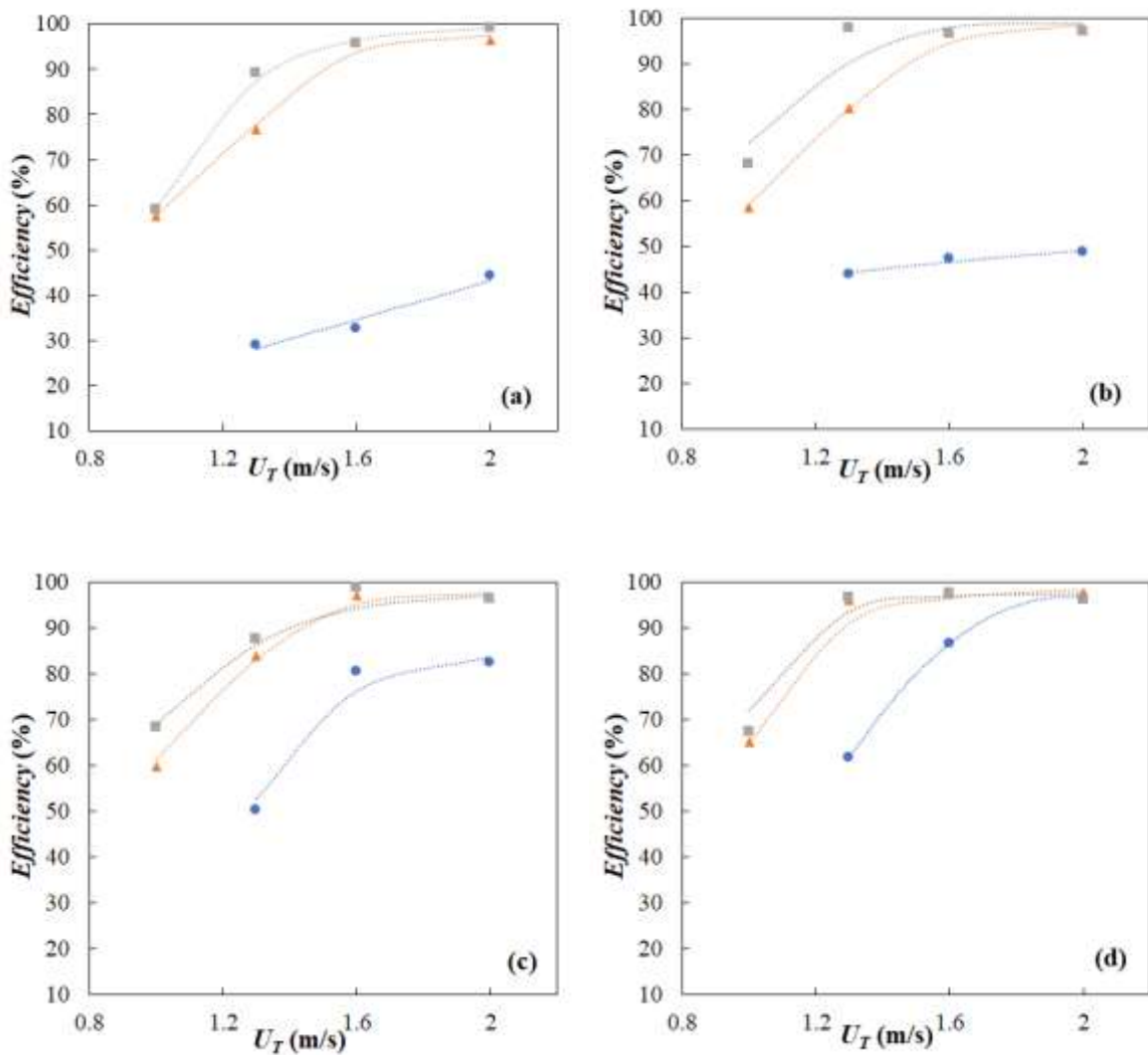
Figure 9: Effect of total superficial flow rate on efficiency for Mn = 80 and $\Phi = 30\%$



● $\Phi = 10\%$ ■ $\Phi = 20\%$ ▲ $\Phi = 30\%$

Figure 10: Effect of gas holdup on efficiency for Mn = 80 and $U_T = 1.6$ m/s

The effect of superficial velocity and gas hold-up was investigated on the overall efficiency of the carbon capture process for the four different mesh geometries. It can be clearly discerned from Figure 11 that as the superficial velocity and gas hold-up increase, the CO₂ removal efficiency increases due to the combined effect of turbulence generated from the high superficial velocity encountered and the insertion of screens with high mesh number. As the multiphase flow passes through the mixers with high mesh number in the turbulently flowing system, bubble breakage becomes dominant and is enhanced leading to a larger interfacial area between the phases. Therefore, the overall removal efficiency increases as the superficial velocity, gas hold-up and mesh number increases.



● $\Phi = 10\%$ ■ $\Phi = 20\%$ ▲ $\Phi = 30\%$

Figure 11: Effect of Superficial velocity and gas holdup on Efficiency:(a) Mn = 30, (b) Mn = 50, (c) Mn = 80 and (d) Mn = 100

D. Energy Requirement

As previously mentioned, the energy requirement is one of the most important decision factors that affect the economic feasibility of a process. The energy requirement can be computed in multiple approaches such as the overall amount of energy supplied to mixer per time, E , the rate of energy dissipation per unit time and mass, ε , and the energy needed to process a unit of the flow mixture, E_{spm} . In this investigation, the term E_{spm} will only be presented as it takes into account the residence time in the reactor (Al Taweel et al., 2007, 2005; Azizi and Al Taweel, 2015; Koglin et al., 1981; Taweel and Walker, 1983).

Pressure drop, total superficial velocity and residence time are the main parameters that affect the specific energy consumption per unit mass, E_{spm} . The higher the pressure drop or total superficial velocity, the higher specific energy consumption rate. Naturally, the higher the energy input into the reactor, the higher the k_{LA} will be due to the increased turbulence. In order to delineate the effect of gas holdup on E_{spm} , *Figure 12* shows the variation of k_{LA} as a function of E_{spm} at different holdups for all mesh geometries. As can be shown, providing larger inputs to the system increased the volumetric mass transfer coefficients. Additionally, it was found that as the holdup increases, the specific energy consumption decreases. This is because the pressure drop decreases (as previously mentioned) while reducing the residence time in the reactor. This is in agreement with the findings of (Azizi and Al Taweel, 2015). Therefore, the

highest E_{spm} value was obtained at the highest superficial velocity ($U_T = 2$ m/s) and lowest gas holdup ($\phi = 10\%$).

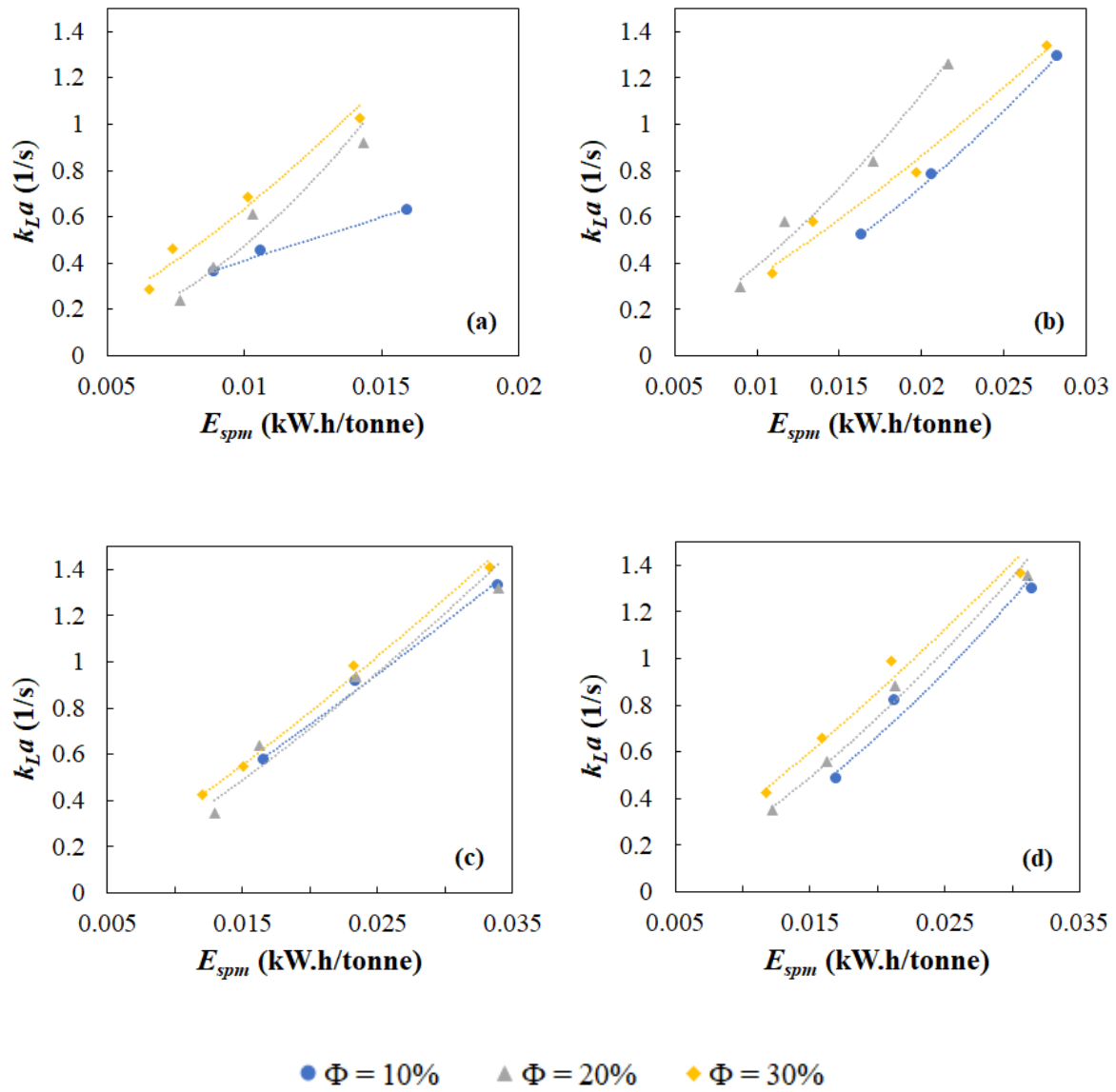


Figure 12: k_{La} versus the energy needed to process a unit of the flowing mixture, E_{spm} ,:(a) Mn = 30, (b) Mn = 50, (c) Mn = 80 and (d) Mn = 100

E. Correlating the volumetric mass transfer coefficient

In this study, two different attempts were made to correlate the volumetric mass transfer coefficient with various operating conditions that affect it such as liquid velocity, gas velocity, gas hold-up and energy input.

When correlating k_{La} to U_L and U_G , the following relation was obtained:

$$k_{La} = 0.0693 \cdot U_L^{1.41} \cdot U_G^{0.48} \cdot (M - b)^{-0.32} \quad [17]$$

This shows that, under the highly turbulent conditions, the liquid velocity has a stronger impact than the gas velocity.

When correlating k_{La} to ε and φ , the following relation was obtained:

$$k_{La} = 0.00628 \cdot \varepsilon^{0.76} \cdot \varphi^{0.35} \quad [18]$$

For both correlations, good agreement between predicted and experimental k_{La} values was obtained. This can be seen in the figures below.

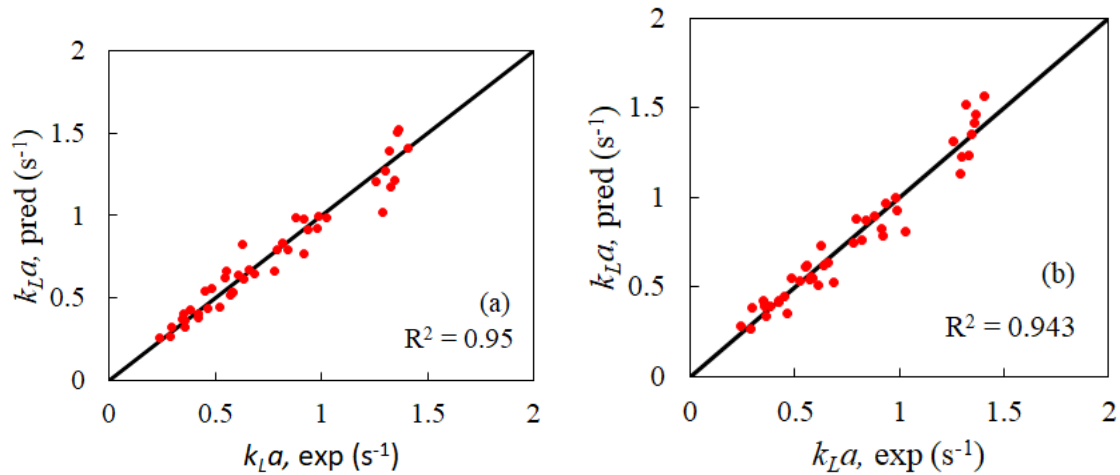


Figure 13: Parity plots for (a): Correlation (17) (b): Correlation (18)

F. Comparison with other gas-liquid contactors used for carbon capture

As can be seen from the results above, the mass transfer characteristics of CO₂ absorption into NaOH can be greatly enhanced upon the insertion of screen-type static mixers into a tubular reactor. A wide range of removal efficiency and volumetric mass transfer coefficient values are obtained depending on the operating parameters and mesh geometry. *Table 4* shows the main criteria that are used to evaluate the mass transfer operation in a certain gas-liquid contactor. It can be clearly seen that the k_{LA} values recorded in the present work were higher than that in a bubble column and comparable to that in a packed bed and rotating packed bed with different packings. On the other hand, removal efficiency was one or two orders of magnitude higher than that of a pyrex batch reactor and was comparable or even slightly higher than that in a packed bed and rotating packed bed.

Table 4: Summary comparison between conventional reactors

Contactor Type	Concentration of CO ₂ injected (% v)	Overall volumetric mass transfer (s ⁻¹)	Removal Efficiency (%)	Source
This work	30	0.1156 – 1.3653	30 – 98	
Bubble column	10 – 12	0.018 – 0.058	30 – 90	Chen et al. (2014)
Packed bed (Structured Packing)	10	0.47 – 1.05		Aroonwilas (1997)
Packed bed with structured packing	4	0.25 – 0.6		Devries (2011)
Pyrex Batch Reactor	30	N/A	10 – 57	Yoo et al. (2013)
Rotating packed bed	10	0.2 – 2.5	10 – 95	Chiang et al. (2017)

Cross flow rotating packed bed	1 – 10	0.3 – 2.54	6.8 – 93	Lin et al. (2011)
Rotating packed bed	1, 10	0.38 – 0.93		Lin et al. (2003)

CHAPTER V

CONCLUSIONS AND RECOMMENDATIONS

Carbon capture intensification was investigated in a tubular reactor equipped with screen-type static mixers at different design and experimental conditions. In this reactor, it was found that the characteristic length of Reynolds number is important in describing the performance of the screen-type static mixers. In other words, not only the diameter of the pipe describes the turbulence across the mixers, but also the wire diameter, mesh size and hydraulic diameter.

The effect of screen geometry gas holdup and superficial velocity were examined on the efficiency of the reactor. As such, the removal efficiency, energy requirement and volumetric mass transfer coefficient were calculated as a function of the previous parameters. For both reactor designs, it was found that k_{LA} increased with an increase in the total superficial velocity as well as gas holdup and reached elevated values of 1.3653 s^{-1} ($U_T = 2 \text{ m/s}$, $\Phi = 30\%$ and $Mn = 100$) at an energy requirement of $0.0306 \text{ kW.h/tonne}$. The efficiency values increased greatly for the screen-type static mixers with higher mesh number revealing that, for the same operating conditions, a reduction in residence time/column height can be realized. In addition to that, the removal efficiency values appeared to increase with the increase in holdup and total superficial velocity for the same screen-type static mixer. This is basically attributed to the generation of high local energy dissipation rate in the region adjacent to the screen, which results in very fine bubble dispersions.

Furthermore, the k_{LA} and efficiency values recorded in the present work were comparable to other volumetric mass transfer coefficient found in the literature, and even one to two orders of magnitude higher in some cases.

Based on the results obtained, it is possible to conclude that:

- Screens having the highest mesh number generated highest $k_L a$ values
- Operating at high velocity and high hold-ups intensified the mass transfer of CO_2 into NaOH and equilibrium was reached at lower residence times
- By tracking the removal efficiency, minimizing the height of the reactor can be realized at such conditions thereby reducing the energy requirement

However, a lot of research should be done to investigate different factors that affect the chemisorption process (concentration of NaOH, untreated water feed, different design conditions, etc..) and better understand the interfacial characteristics (interfacial area) that are of primary importance for the mass transfer operation.

BIBLIOGRAPHY

- Abou Hweij, K., Azizi, F., 2015. Hydrodynamics and residence time distribution of liquid flow in tubular reactors equipped with screen-type static mixers. *Chem. Eng. J.* 279, 948–963.
- Al Taweel, A.M., Azizi, F., Sirijeerachai, G., 2013. Static mixers: Effective means for intensifying mass transfer limited reactions. *Chem. Eng. Process. Process Intensif.* 72, 51–62.
- Al Taweel, A.M., Li, C., Gomaa, H.G., Yuet, P., 2007. Intensifying mass transfer between immiscible liquids: Using screen-type static mixers. *Chem. Eng. Res. Des.* 85, 760–765.
- Al Taweel, A.M., Yan, J., Azizi, F., Odedra, D., Gomaa, H.G., 2005. Using in-line static mixers to intensify gas-liquid mass transfer processes. *Chem. Eng. Sci.* 60, 6378–6390.
- Altaweel, A., 1996. A Novel Static Mixer for the Effective Dispersion of Immiscible Liquids. *Chem. Eng. Res. Des.* 74, 445–450.
- Andersson, R., Andersson, B., Chopard, F., Norén, T., 2004. Development of a multi-scale simulation method for design of novel multiphase reactors. *Chem. Eng. Sci.* 59, 4911–4917.
- Aroonwilas, A., 2001. MASS-TRANSFER WITH CHEMICAL REACTION IN STRUCTURED PACKING FOR CO₂ ABSORPTION PROCESS A.
- Aroonwilas, A., Veawab, A., Tontiwachwuthikul, P., 1999. Behavior of the Mass-Transfer Coefficient of Structured Packings in CO₂ Absorbers with Chemical Reactions. *Ind. Eng. Chem. Res.* 38, 2044–2050.
- Azizi, F., Al Taweel, A.M., 2015. Mass Transfer in an Energy-Efficient High-Intensity Gas-

- Liquid Contactor. *Ind. Eng. Chem. Res.* 54, 11635–11652.
- Azizi, F., Hweij, K.A., 2017. Liquid-Phase Axial Dispersion of Turbulent Gas – Liquid Co-Current Flow Through Screen-Type Static Mixers 63.
- Azizi, F., Taweel, A.M.A., 2011. Turbulently flowing liquid-liquid dispersions. Part I: Drop breakage and coalescence. *Chem. Eng. J.* 166, 715–725.
- Bhosale, R.R., Kumar, A., Almomani, F., Ghosh, U., Alnouss, A., Scheffe, J., Gupta, R.B., 2016. CO₂Capture Using Aqueous Potassium Carbonate Promoted by Ethylaminoethanol: A Kinetic Study. *Ind. Eng. Chem. Res.* 55, 5238–5246.
- Bourne, J.R., Lips, M., 1991. Micromixing in grid-generated turbulence: Theoretical analysis and experimental study. *Chem. Eng. J.* 47, 155–162.
- Budzyński, P., Gwiazda, A., Dziubiński, M., 2017. Intensification of mass transfer in a pulsed bubble column. *Chem. Eng. Process. Process Intensif.* 112, 18–30.
- Cents, A.H.G., De Bruijn, F.T., Brilman, D.W.F., Versteeg, G.F., 2005. Validation of the Danckwerts-plot technique by simultaneous chemical absorption of CO₂ and physical desorption of O₂. *Chem. Eng. Sci.* 60, 5809–5818.
- Chen, P.C., Huang, C.F., Chen, H.W., Yang, M.W., Tsao, C.M., 2014. Capture of CO₂ from coal-fired power plant with NaOH solution in a continuous pilot-scale bubble-column scrubber. *Energy Procedia* 61, 1660–1664.
- Chen, P.C., Liao, C., 2014. A Study on CO₂ Absorption in Bubble Column Using DEEA/EEA Mixed Solvent. *Int. J. Eng. Pract. Res.* 3, 78–82.
- Chen, P.C., Luo, Y.X., Cai, P.W., 2015. CO₂Capture Using Monoethanolamine in a Bubble-Column Scrubber. *Chem. Eng. Technol.* 38, 274–282.

- Chen, P.C., Shi, W., Du, R., Chen, V., 2008. Scrubbing of CO₂ greenhouse gases, accompanied by precipitation in a continuous bubble-column scrubber. *Ind. Eng. Chem. Res.* 47, 6336–6343.
- Chiang, C.-Y., Lee, D.-W., Liu, H.-S., 2017. Carbon dioxide capture by sodium hydroxide-glycerol aqueous solution in a rotating packed bed. *J. Taiwan Inst. Chem. Eng.* 72, 29–36.
- Couchaux, G., Barth, D., Jacquin, M., Faraj, A., Grandjean, J., 2014. Kinetics of Carbon Dioxide with Amines. I. Stopped-Flow Studies in Aqueous Solutions. A Review. *Oil Gas Sci. Technol. – Rev. d'IFP Energies Nouv.* 69, 865–884.
- Crossno, S.K., Kalbus, L.H., Kalbus, G.E., 1996. Determination of Carbon Dioxide by Titration.
- Devries, N.P., 2014. CO₂ Absorption into Concentrated Carbonate solutions with promoters at elevated temperatures. *Environ. Regul.*
- Drăgan, S., 2016. Calculation of the effective mass transfer area in turbulent contact absorber. *Stud. Univ. Babeş-Bolyai Chem.* 61, 227–238.
- Duss, M., Meierhofer, H., Nutter, D.E., 2001. Effective interfacial area and liquid holdup of Nutter Rings at high liquid loads. *Chem. Eng. Technol.* 24, 716–723.
- El-Ali, M.S., 2001. Performance Characteristics of a novel liquid-liquid contactor.
- Ferreira, B.S., Fernandes, H.L., Reis, A., Mateus, M., 1998. Microporous hollow fibres for carbon dioxide absorption: Mass transfer model fitting and the supplying of carbon dioxide to microalgal cultures. *J. Chem. Technol. Biotechnol.* 71, 61–70.
- Fleischer, C., Becker, S., Eigenberger, G., 1996. Detailed modeling of the chemisorption of

- CO₂ into NaOH in a bubble column. *Chem. Eng. Sci.* 51, 1715–1724.
- Gabrielsen, J., Svendsen, H.F., Michelsen, M.L., Stenby, E.H., Kontogeorgis, G.M., 2007. Experimental validation of a rate-based model for CO₂ capture using an AMP solution. *Chem. Eng. Sci.* 62, 2397–2413.
- Gavini, S., 2017. MASS TRANSFER AND PROCESS CONTROL IN RANDOMLY PACKED COLUMN A CASE STUDY ON CO₂ ABSORPTION WITH NaOH A THESIS Presented to the Department of Chemical Engineering California State University, Long Beach In Partial Fulfillment of the Requirements for the D.
- Gavrilescu, M., Tudose, R.Z., 1995. Intensification of transfer processes in biotechnology and chemical engineering using static mixers. (Review). *Acta Biotechnol.* 15, 3–26.
- Ghanem, A., Lemenand, T., Della Valle, D., Peerhossaini, H., 2014. Static mixers: Mechanisms, applications, and characterization methods - A review. *Chem. Eng. Res. Des.* 92, 205–228.
- Guo, Y., Niu, Z., Lin, W., 2011. Comparison of removal efficiencies of carbon dioxide between aqueous ammonia and NaOH solution in a fine spray column. *Energy Procedia* 4, 512–518.
- Heyouni, a, Roustan, M., Do-quang, Z., 2002. Hydrodynamics and mass transfer in gas – liquid flow through static mixers. *Chem. Eng. Sci.* 57, 3325–3333.
- Hikita, H., Asai, S., Takatsuka, T., 1976. Absorption of carbon dioxide into aqueous sodium hydroxide and sodium carbonate-bicarbonate solutions. *Chem. Eng. J.* 11, 131–141.
- Hu, G., Nicholas, N.J., Smith, K.H., Mumford, K.A., Kentish, S.E., Stevens, G.W., 2016. Carbon dioxide absorption into promoted potassium carbonate solutions: A review. *Int.*

- J. Greenh. Gas Control 53, 28–40.
- Isa, F., Zabiri, H., Ng, N.K.S., Shariff, A.M., 2018. Purification of CO₂ removal via promoted potassium carbonate: A review on modelling & simulation techniques. *Int. J. Greenh. Gas Control* 76, 236–265.
- Iso, Y., Huang, J., Kato, M., Matsuno, S., Takano, K., 2013. Numerical and experimental study on liquid film flows on packing elements in absorbers for post-combustion CO₂ capture. *Energy Procedia* 37, 860–868.
- Jain, D., Kuipers, J.A.M., Deen, N.G., 2015. Numerical modeling of carbon dioxide chemisorption in sodium hydroxide solution in a micro-structured bubble column. *Chem. Eng. Sci.* 137, 685–696.
- Kato, M., Nakagawa, K., Essaki, K., Maezawa, Y., Takeda, S., Kogo, R., Hagiwara, Y., 2005. Novel CO₂ absorbents using lithium-containing oxide. *Int. J. Appl. Ceram. Technol.* 2, 467–475.
- Kim, D.M., Cho, J., 2011. A comparative study of carbon dioxide capture capabilities between methanol solvent and aqueous monoethanol amine solution. *Korean J. Chem. Eng.* 28, 22–26.
- Kim, Y.E., Lim, J.A., Jeong, S.K., Yoon, Y. Il, Bae, S.T., Nam, S.C., 2013. Comparison of carbon dioxide absorption in aqueous MEA, DEA, TEA, and AMP solutions. *Bull. Korean Chem. Soc.* 34, 783–787.
- Koglin, B., Pawlowski, J., Schnoring, H., 1981. Kontinuierliches Emulgieren mit Rotor/Stator-Maschinen: Einfluss der volumenbezogenen Dispergierleistung und der Verweilzeit auf die Emulsionsfeinheit. *Chemie Ing. Tech.* 53, 641–647.

- Kordylewski, W., Sawicka, D., Falkowski, T., 2013. Laboratory tests on the efficiency of carbon dioxide capture from gases in NaOH solutions. *J. Ecol. Eng.* 14, 54–62.
- Koronaki, I.P., Prentza, L., Papaefthimiou, V.D., 2017. Parametric analysis using AMP and MEA as aqueous solvents for CO₂ absorption. *Energy* 110, 126–135.
- Kothandaraman, A., Nord, L., Bolland, O., Herzog, H.J., McRae, G.J., 2009. Comparison of solvents for post-combustion capture of CO₂ by chemical absorption. *Energy Procedia* 1, 1373–1380.
- Krauß, M., Rzehak, R., 2017. Reactive absorption of CO₂ in NaOH: Detailed study of enhancement factor models. *Chem. Eng. Sci.* 166, 193–209.
- Kumar, S., Cho, J.H., Moon, I., 2014. Ionic liquid-amine blends and CO₂BOLs: Prospective solvents for natural gas sweetening and CO₂ capture technology-A review. *Int. J. Greenh. Gas Control* 20, 87–116.
- Laakkonen, M., Alopaeus, V., Aittamaa, J., 2006. Validation of bubble breakage, coalescence and mass transfer models for gas-liquid dispersion in agitated vessel. *Chem. Eng. Sci.* 61, 218–228.
- Li, W., Zhao, X., Liu, B., Tang, Z., 2014. Mass Transfer Coefficients for CO₂ Absorption into Aqueous Ammonia Using Structured Packing. *Ind. Eng. Chem. Res.* 53, 6185–6196.
- Lin, C.-C., Liu, W.-T., Tan, C.-S., 2003. Removal of Carbon Dioxide by Absorption in a Rotating Packed Bed. *Ind. Eng. Chem. Res.* 42, 2381–2386.
- Lin, C.C., Kuo, Y.W., 2016. Mass transfer performance of rotating packed beds with blade packings in absorption of CO₂ into MEA solution. *Int. J. Heat Mass Transf.* 97, 712–

718.

- Luo, Y., Chu, G.W., Zou, H.K., Wang, F., Xiang, Y., Shao, L., Chen, J.F., 2012a. Mass transfer studies in a rotating packed bed with novel rotors: Chemisorption of CO₂. *Ind. Eng. Chem. Res.* 51, 9164–9172.
- Luo, Y., Chu, G.W., Zou, H.K., Zhao, Z.Q., Dudukovic, M.P., Chen, J.F., 2012b. Gas-liquid effective interfacial area in a rotating packed bed. *Ind. Eng. Chem. Res.* 51, 16320–16325.
- Luo, Y., Luo, J.Z., Chu, G.W., Zhao, Z.Q., Arowo, M., Chen, J.F., 2017. Investigation of effective interfacial area in a rotating packed bed with structured stainless steel wire mesh packing. *Chem. Eng. Sci.* 170, 347–354.
- MacDowell, N., Florin, N., Buchard, A., Hallett, J., Galindo, A., Jackson, G., Adjiman, C.S., Williams, C.K., Shah, N., Fennell, P., 2010. An overview of CO₂ capture technologies. *Energy Environ. Sci.* 3, 1645–1669.
- Mandal, A., Kundu, G., Mukherjee, D., 2008. Interfacial Area and Liquid-Side Volumetric Mass Transfer Coefficient in a Downflow Bubble Column. *Can. J. Chem. Eng.* 81, 212–219.
- Mandal, B.P., Guha, M., Biswas, A.K., Bandyopadhyay, S.S., 2001. Removal of carbon dioxide by absorption in mixed amines: Modelling of absorption in aqueous MDEA/MEA and AMP/MEA solutions. *Chem. Eng. Sci.* 56, 6217–6224.
- Merchuk, J.C., 1980. Mass transfer characteristics of a column with small plastic packings. *Chem. Eng. Sci.* 35, 743–745.
- Munter, R., 2010. Comparison of Mass Transfer Efficiency and Energy Consumption in

- Static Mixers. *Ozone Sci. Eng.* 32, 399–407.
- Nair, P.S., Selvi, P.P., 2014. Absorption of Carbon dioxide in Packed Column. *Int. J. Sci. Res. Publ.* 4, 2250–3153.
- Niu, Z., Guo, Y., Lin, W., 2009. Experimental studies on CO₂ capture in a spray scrubber using NaOH solution. *2009 Int. Conf. Energy Environ. Technol. ICEET 2009* 3, 52–55.
- Olajire, A.A., 2010. CO₂ capture and separation technologies for end-of-pipe applications - A review. *Energy* 35, 2610–2628.
- Olivier, J.G.J., Schure, K.M., Peters, J.A.H.W., 2017. TRENDS IN GLOBAL CO₂ AND TOTAL GREENHOUSE GAS EMISSIONS 2017 Report Trends in global CO₂ and total greenhouse gas emissions: 2017 Report.
- Oyevaar, M., Zijl, A., Westerterp, R., 1988. Interfacial areas and gas hold-ups at elevated pressures in a mechanically agitated gas-liquid reactor. *Chem. Eng. Technol.* 11, 1–10.
- Oyevaar, M.H., Westerterp, K.R., 1989. The use of the chemical method for the determination of interfacial areas in gas-liquid contactors. *Chem. Eng. Sci.* 44, 2691–2701.
- Pangarkar, V.G., 2017. Process intensification in multiphase reactors: From concept to reality. *Chem. Eng. Process. Process Intensif.* 120, 1–8.
- Phan, D.T., Maeder, M., Burns, R.C., Puxty, G., 2015. Catalysis of CO₂ absorption in aqueous solution by vanadate and sulfate and their application to post combustion capture. *Int. J. Greenh. Gas Control* 36, 60–65.
- Pohorecki, R., Moniuk, W., 1988. Kinetics of reaction between carbon dioxide and hydroxyl ions in aqueous electrolyte solutions. *Chem. Eng. Sci.* 43, 1677–1684.

- Powell, C.E., Qiao, G.G., 2006. Polymeric CO₂/N₂ gas separation membranes for the capture of carbon dioxide from power plant flue gases. *J. Memb. Sci.* 279, 1–49.
- Rajan, S., Kumar, M., Ansari, M.J., Rao, D.P., Kaistha, N., 2011. Limiting Gas-Liquid Flows and Mass Transfer in a Novel Rotating Packed Bed (HiGee). *Ind. Eng. Chem. Res.* 50, 986–997.
- Reay, D., Ramshaw, C., Harvey, A., 2008. *Process Intensification - Engineering for Efficiency, Sustainability and Flexibility* - Knovel. Elsevier.
- Rezazadeh, F., Gale, W.F., Rochelle, G.T., Sachde, D., 2017. Effectiveness of absorber intercooling for CO₂ absorption from natural gas fired flue gases using monoethanolamine solvent. *Int. J. Greenh. Gas Control* 58, 246–255.
- Saeed, I.M., Alaba, P., Mazari, S.A., Basirun, W.J., Lee, V.S., Sabzoi, N., 2018. Opportunities and challenges in the development of monoethanolamine and its blends for post-combustion CO₂ capture. *Int. J. Greenh. Gas Control* 79, 212–233.
- Samanta, A., Zhao, A., Shimizu, G.K.H., Sarkar, P., Gupta, R., 2012. Post-Combustion CO₂ Capture Using Solid Sorbents: A Review. *Ind. Eng. Chem. Res.* 51, 1438–1463.
- Shekhawat, D., Luebke, D.R., Pennline, H.W., 2003. A review of carbon dioxide selective membranes. *US Dep. energy* 1200, 9–11.
- Shen, S., Feng, X., Zhao, R., Ghosh, U.K., Chen, A., 2013. Kinetic study of carbon dioxide absorption with aqueous potassium carbonate promoted by arginine. *Chem. Eng. J.* 222, 478–487.
- Shen, S., Yang, Y., 2016. *Carbon Dioxide Absorption into Aqueous Potassium Salt Solutions of Arginine for Post-Combustion Capture*.

- Skoczylas, A., Majewski, W., 1991. Effective interfacial area in mechanical thin-layer apparatus. *Chem. Eng. J.* 46, 69–78.
- Spigarelli, B.P., 2013. A NOVEL APPROACH TO CARBON DIOXIDE CAPTURE AND STORAGE.
- Tavan, Y., Hossein, S., 2017. A novel rate of the reaction between NaOH with CO₂ at low temperature in spray dryer. *Petroleum* 3, 51–55.
- Taweel, A.M.A., Walker, L.D., 1983. Liquid dispersion in static in-line mixers. *Can. J. Chem. Eng.* 61, 527–533.
- Thakur, R.K., Vial, C., Nigam, K.D.P., Nauman, E.B., Djelveh, G., 2003. Static mixers in the process industries - a review. *Chem. Eng. Res. Des.* 81, 787–826.
- Thee, H., Smith, K.H., Silva, G. da, Kentish, S.E., Stevens, G.W., 2015. Carbonic anhydrase promoted absorption of CO₂ into potassium carbonate solutions. *Greenh. Gases Sci. Technol.* 2, 108*114.
- Thee, H., Suryaputradinata, Y.A., Mumford, K.A., Smith, K.H., Silva, G. da, Kentish, S.E., Stevens, G.W., 2012. A kinetic and process modeling study of CO₂ capture with MEA-promoted potassium carbonate solutions. *Chem. Eng. J.* 210, 271–279.
- Thiruvalluvan Sujatha, K., Jain, D., Kamath, S., Kuipers, J.A.M., Deen, N.G., 2017. Experimental and numerical investigation of a micro-structured bubble column with chemisorption. *Chem. Eng. Sci.* 169, 225–234.
- Tsai, C.Y., Chen, Y.S., 2015. Effective interfacial area and liquid-side mass transfer coefficients in a rotating bed equipped with baffles. *Sep. Purif. Technol.* 144, 139–145.
- Turunen, I., Haario, H., 1995. Mass Transfer in Tubular Static Reactors Mixers Equipped

With 49, 5257–5269.

UNEP, n.d. The Emissions Gap Report 2017 A UN Environment Synthesis Report.

Vaidya, P.D., Kenig, E.Y., 2007. CO₂-alkanolamine reaction kinetics: A review of recent studies. *Chem. Eng. Technol.* 30, 1467–1474.

Vázquez, G., Cancela, M.A., Riverol, C., Alvarez, E., Navaza, J.M., 2000. Determination of interfacial areas in a bubble column by different chemical methods. *Ind. Eng. Chem. Res.* 39, 2541–2547.

Versteeg, G.F., VAN DIJCK, L.A.J., VAN SWAAIJ, W.P.M., 1996. ON THE KINETICS BETWEEN CO₂ AND ALKANOLAMINES BOTH IN AQUEOUS AND NON-AQUEOUS SOLUTIONS. AN OVERVIEW. *Chem. Eng. Commun.* 144, 113–158.

Wang, C., Perry, M., Seibert, F., Rochelle, G.T., 2013. Characterization of novel structured packings for CO₂ capture 37, 2145–2153.

Wang, X., Conway, W., Burns, R., McCann, N., Maeder, M., 2010. Comprehensive study of the hydration and dehydration reactions of carbon dioxide in aqueous solution. *J. Phys. Chem. A* 114, 1734–1740.

Weiland, R.H., Ahlgren, K.R., Evans, M., 1993. Mass-Transfer Characteristics of Some Structured Packings. *Ind. Eng. Chem. Res.* 32, 1411–1418.

Xu, X., Song, C., Miller, B.G., Scaroni, A.W., 2005. Adsorption separation of carbon dioxide from flue gas of natural gas-fired boiler by a novel nanoporous “molecular basket” adsorbent. *Fuel Process. Technol.* 86, 1457–1472.

Yang, H., Xu, Z., Fan, M., Gupta, R., Slimane, R.B., Bland, A.E., Wright, I., 2008. Progress in carbon dioxide separation and capture: A review. *J. Environ. Sci.* 20, 14–27.

- Yang, K., Chu, G., Zou, H., Sun, B., Shao, L., Chen, J.F., 2011. Determination of the effective interfacial area in rotating packed bed. *Chem. Eng. J.* 168, 1377–1382.
- Yoo, M., Han, S.-J., Wee, J.-H., 2013. Carbon dioxide capture capacity of sodium hydroxide aqueous solution. *J. Environ. Manage.* 114, 512–519.
<https://doi.org/10.1016/j.jenvman.2012.10.061>
- Yoshida, F., Miura, Y., 1963. Effective interfacial area in packed columns for absorption with chemical reaction. *AIChE J.* 9, 331–337.
- Yue, J., Chen, G., Yuan, Q., Luo, L., Gonthier, Y., 2007. Hydrodynamics and mass transfer characteristics in gas-liquid flow through a rectangular microchannel. *Chem. Eng. Sci.* 62, 2096–2108.
- Ziókowski, D., Morawski, J., 1987. The flow characteristic of the liquid streams inside a tubular apparatus equipped with static mixing elements of a new type. *Chem. Eng. Process.* 21, 131–139.

APPENDIX I

SUPPLEMENTARY FIGURES

A. Pressure drop measurements

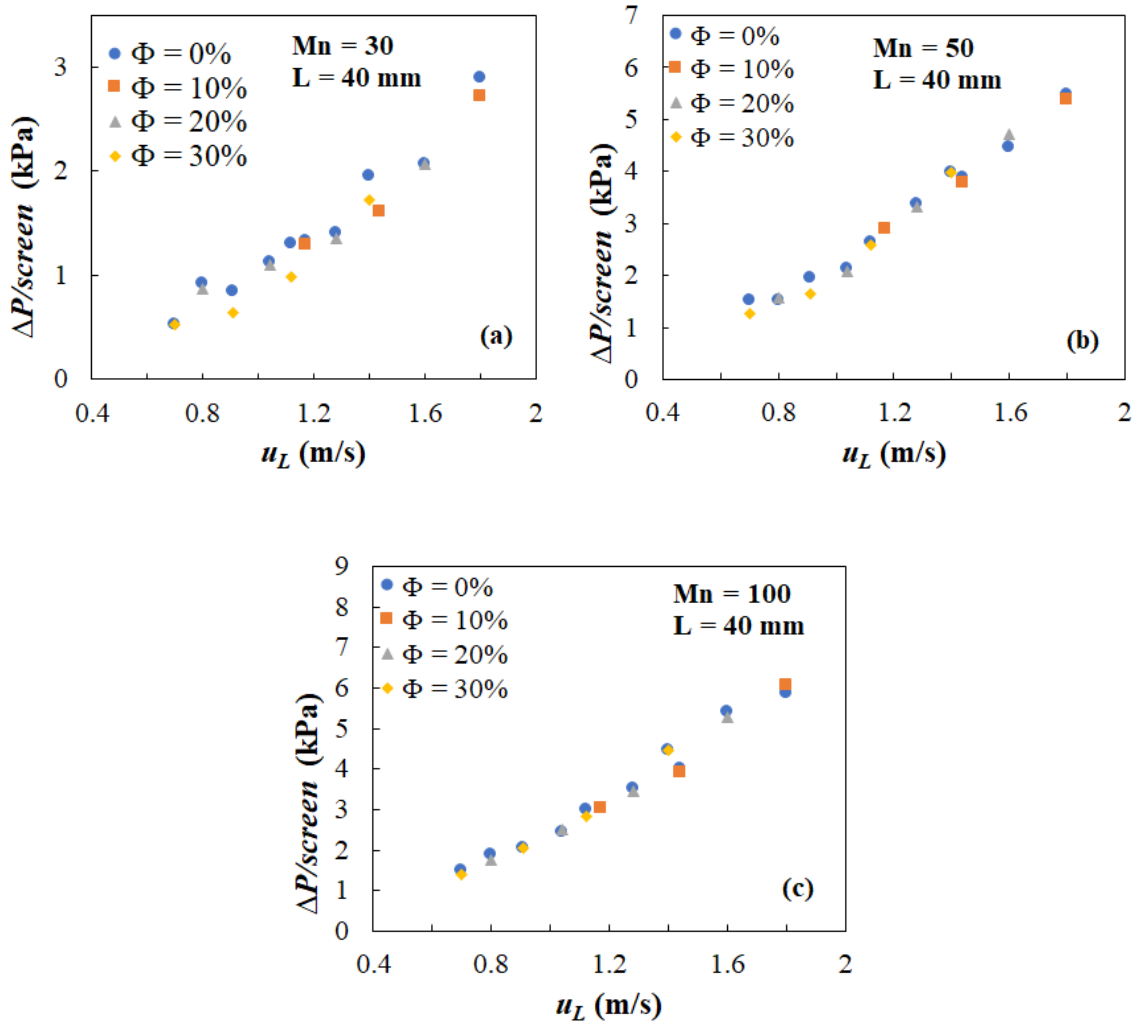


Figure 14: Effect of gas holdup and superficial liquid velocity on the pressure drop per screen: (a) Mesh 30, (b) Mesh 50 and (c) Mesh 100

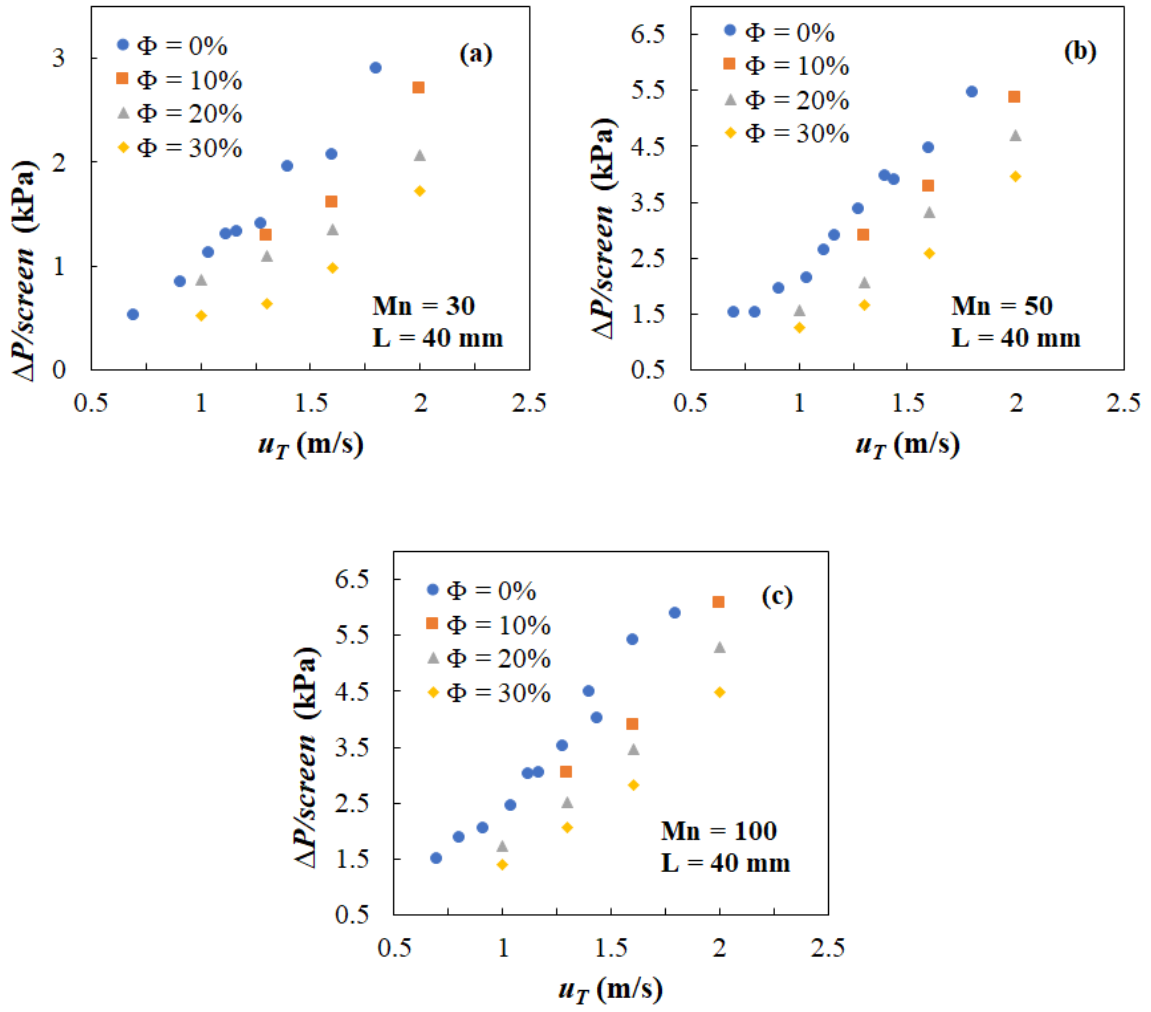
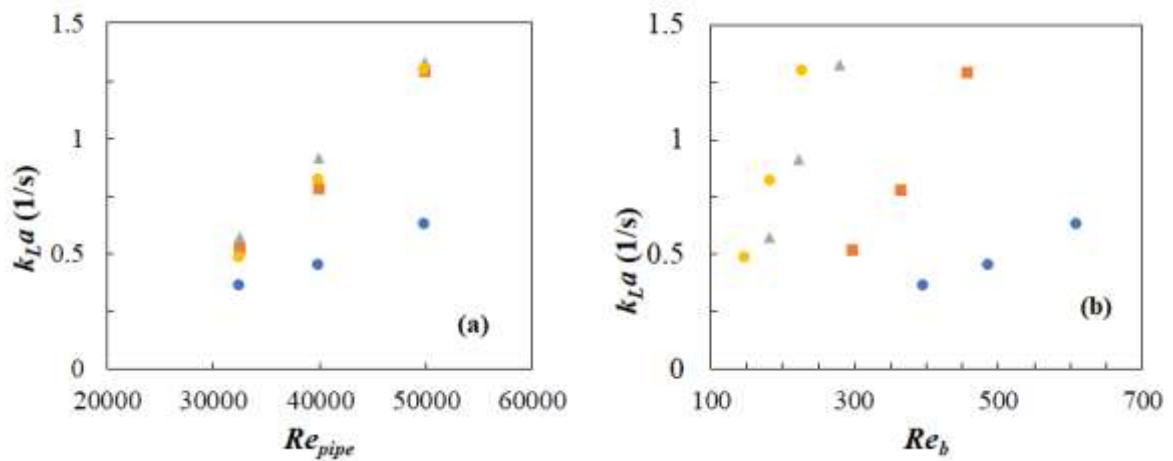


Figure 15: Effect of gas holdup and total superficial velocity on pressure drop per screen: (a) Mesh 30, (b) Mesh 50 and (c) Mesh 100

B. Volumetric Mass transfer coefficient



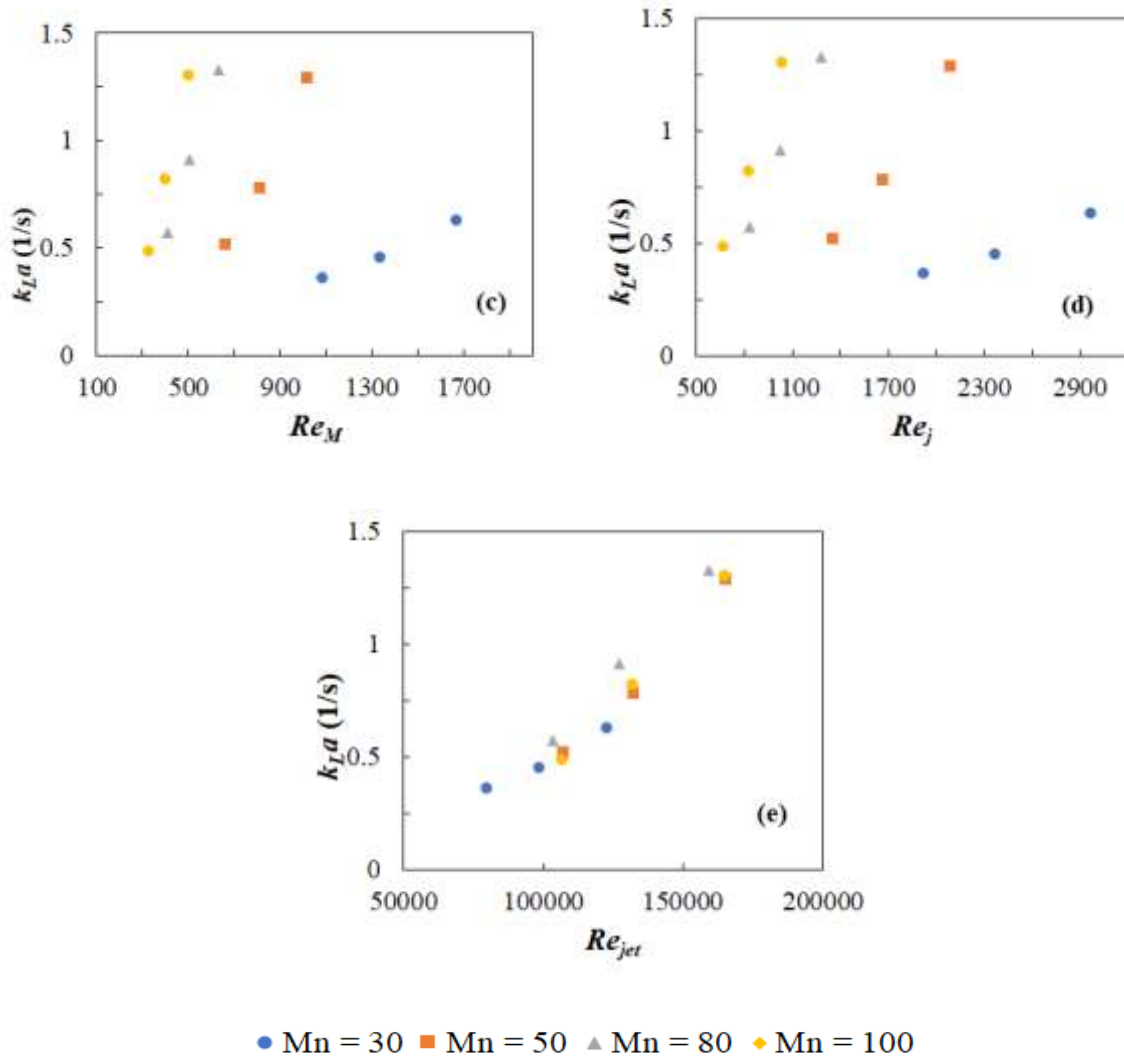
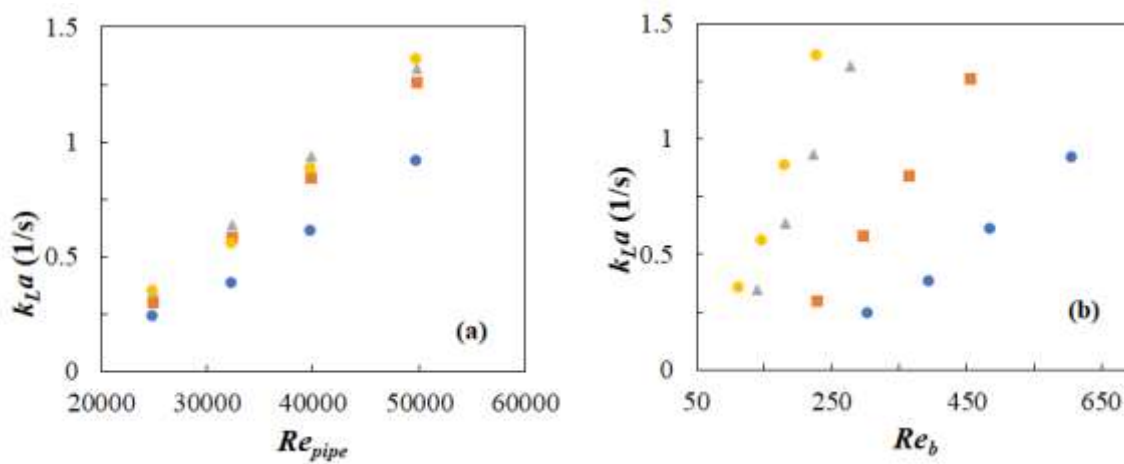


Figure 16: The variation of k_{La} with Reynolds number for all four screen geometries ($\varphi = 10\%$): (a) Re_{pipe} , (b) Re_b , (c) Re_M , (d) Re_j and (e) Re_{jet}



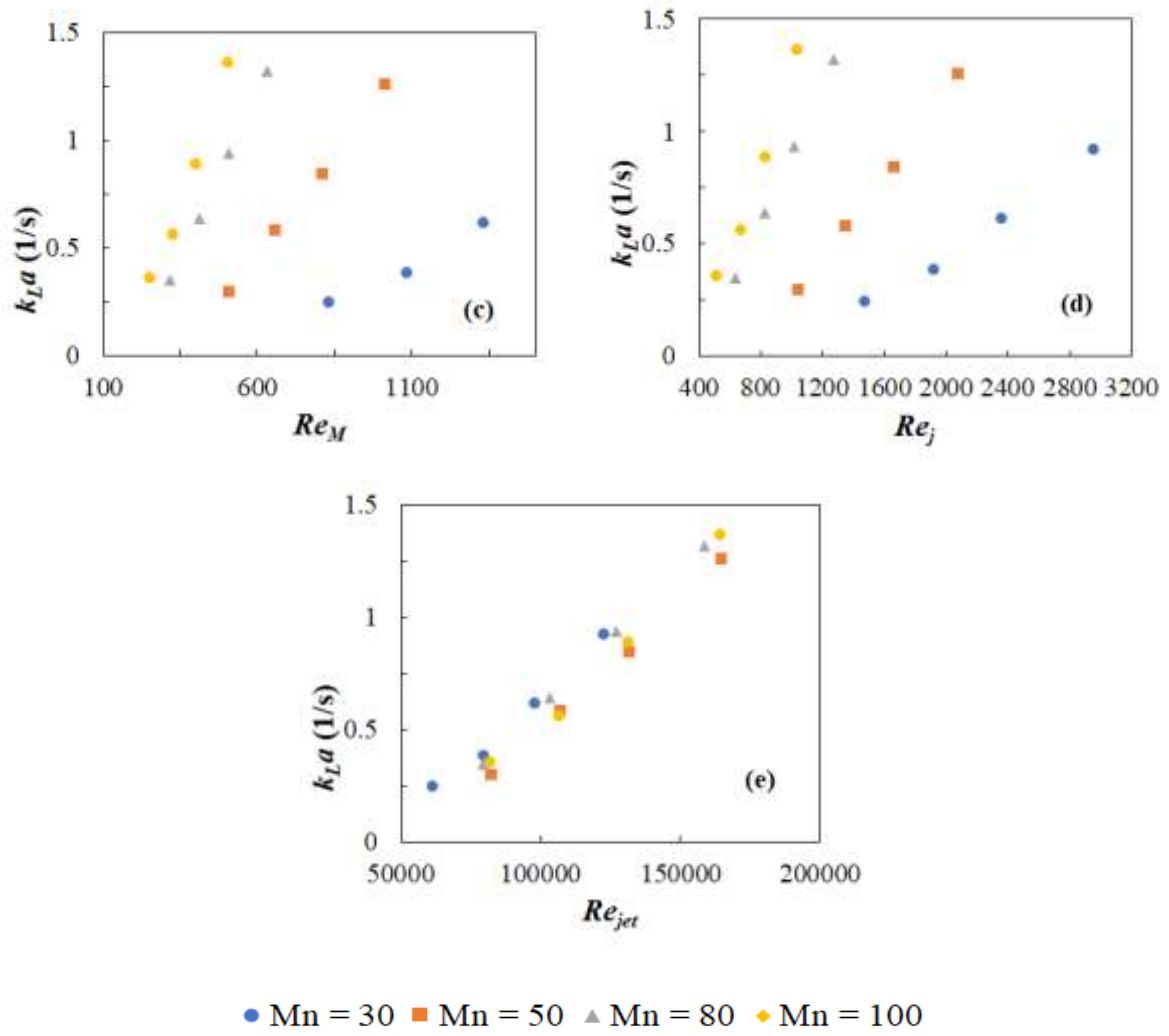


Figure 17: The variation of k_{La} with Reynolds number for all four screen geometries ($\phi = 20\%$): (a) Re_{pipe} , (b) Re_b , (c) Re_M , (d) Re_j and (e) Re_{jet}

APPENDIX II

Raw Data Experiments

In the results below, P represents the first equivalence point in mL and T represents the second equivalence point in mL according to the standard titration method. P_{in} and P_{out} represents the pressure at the inlet and outlet in bar, and U_T is the total superficial velocity in m/s.

1. $Mn = 30$, $\varphi = 10\%$

U_T	1		1.3		1.6		2	
P_{in}			1.58535714		1.74829932		1.84039287	
P_{out}			1.31653571		1.421768707		1.323428571	
Sample	P	T	P	T	P	T	P	T
0			127	131	95.75	98.7	70	72.3
1			132.8	136.9	106.3	109.5	62.15	64.8
2			133	137.3	109.25	112.6	64.55	67.6
3			137.9	142.5	106.45	110	63	66.6
4			138.6	143.3	103.2	107.05	62.15	65.85
5			142.2	147	109.2	113	64.4	68
6			139.8	144.7	106.6	110.45	66.35	69.95
7			141.3	146.1	110.9	114.8	66.3	70

2. $Mn = 30$, $\varphi = 20\%$

U_T	1	1.3	1.6	2
P_{in}	1.476190476	1.578464286	1.70535714	1.709428571

P_{out}	1.258503401		1.323428571		1.406142857		1.295857143	
Sample	P	T	P	T	P	T	P	T
0	126.2	129.7	107.1	110.25	106	109.3	121	124.75
1	124.2	128	99.8	103.35	101.45	105.15	117.8	122.2
2	125.5	129.5	99.2	102.95	100.45	104.8	116.1	121.6
3	125.5	130.5	98.8	105.15	97.85	105.4	113	121
4	123.7	129.5	97.2	104.4	93.5	102.45	115.3	126.5
5	124.4	130	97.4	104.4	90.25	99.3	117.3	128.3
6	122.5	129.35	93.8	101	92.5	102	112	121.5
7	122.2	129.2	93.8	101.4	88.9	98.5	108	118

3. $Mn = 30, \varphi = 30\%$

U_T	1		1.3		1.6		2	
P_{in}	1.419928571		1.461285714		1.612928571		1.840392857	
P_{out}	1.2545		1.275178571		1.357892857		1.426821429	
Sample	P	T	P	T	P	T	P	T
0	83	86.3	163.2	167.7	125.85	129.6	123	127.1
1	77.9	82	126	131.75	110.85	115.75	119.5	125
2	76.8	81.6	122.2	128.85	108.5	114.35	123	129.4
3	75	81.6	109.25	120.4	98.6	109	102.6	114.6

4	75.7	82.7	118	131.9	104	115.9	97.8	109.9
5	71.8	84	118	132.35	100	113	95	108
6	74.2	84.4	120.5	135.35	95	109	90.5	105
7	72	82.8	119.9	135.75	98.8	113	90.5	106.1

4. $Mn = 50$, $\varphi = 10\%$

U_T	1		1.3		1.6		2	
P_{in}			1.840392857		2.04717857		2.081642857	
P_{out}			1.3096426		1.37857143		1.164892857	
Sample	P	T	P	T	P	T	P	T
0			82.1	85	s	95.25	49.9	52.7
1			92.15	95.35	95.6	99.45	56.1	59.3
2			92.85	96.2	95.8	100	54.5	58.25
3			88.2	92.1	96.5	101	54.85	59.25
4			87.45	91.45	94.2	98.9	55.5	59.8
5			93.3	97.3	94.1	98.5	54	58.2
6			91	95.1	91	96	51.3	55.6
7			91.85	96.2	93.2	98.25	54	58.4

5. $Mn = 50$, $\varphi = 20\%$

U_T	1	1.3	1.6	2
-------	---	-----	-----	---

P_{in}	1.564678571		1.68875		1.97825		1.88642857	
P_{out}	1.2545		1.295857143		1.385464286		1.123535714	
Sample	P	T	P	T	P	T	P	T
0	71	73.3	86.05	89.25	96	99.1	79.2	82.5
1	72.6	75.4	80.65	85	92.75	96.6	67.2 5	71.4 5
2	71.7	74.65	77.95	82.8	92.3	97.85	64.9	70.0 5
3	69.05	74.4	70.55	78	86.35	94	62.7 5	69.1 5
4	70.4	75.7	76.45	85	89.3	99	69	78
5	65.15	70.2	76.1	84.5	86.05	96	71	80.5
6	65	71.5	76.9	86	87.9	97.8	67.9 5	78
7	61.5	68.1	74.35	83.5	86.5	96.75	64	74.2

6. $Mn = 50, \varphi = 30\%$

U_T	1		1.3		1.6		2	
P_{in}	1.49575		1.612928571		1.840392857		2.185035714	
P_{out}	1.220035714		1.2545		1.344107143		1.48857143	
Sample	P	T	P	T	P	T	P	T
0	143.15	147.1	102.5	105.2	74.75	79.5	3.533 3	3.9
1	133.5	138.45	97	101.9	69.05	76.9	83	87.2

2	139.05	145.4	98.25	103.25	65.95	77.15	84.1	89.8
3	134.25	144	87	95	54.9	70	78	85.4
4	133.2	143.2	93.5	102.2	62.3	78	74.25	86.7 5
5	132.4	145.65	87.5	102	62	78.05	72.5	85.7
6	136.5	147.3	91	104	62.45	80	75	90
7	133.5	146	85	100	56.55	74	70.15	86

7. $Mn = 80$, $\varphi = 10\%$

U_T	1		1.3		1.6		2	
P_{in}			2.047178571		2.116107		2.322892	
P_{out}			1.509535714		1.357892		1.2889642	
Sample	P	T	P	T	P	T	P	T
0			106.1	110.15	70.1	72.75	57.6	60
1			115.95	120.4	81.3	84.6	63.9	67
2			118.35	123.1	83.45	86.95	66.7	70.35
3			118	123.4	85	89.05	65.2	69.7
4			124.55	129.9	94.7	99.1	58.5	63.1
5			125.75	131.35	99.2	104.05	54.7	59.7
6			115.6	121.3	98.8	103.75	55.7	60.8
7			119.25	124.9	99.95	105	62.3	67.2

8. $Mn = 80$, $\varphi = 20\%$

U _T	1		1.3		1.6		2	
P _{in}	1.66807		1.97825		2.116107		2.495214	
P _{out}	1.295857		1.45439		1.440607		1.413035	
Sample	P	T	P	T	P	T	P	T
0	93.3	96.55	124	127.45	97.7	100.2	69.9	72.5
1	84.8	88.65	117	121.55	96.8	100.65	67.55	72
2	88.25	92.2	118.6	123.8	105.15	110.1	54.5	60
3	83.75	90	109.95	117.6	99.7	106.85	51.85	59.6 5
4	88.6	95	113.8	122.6	96.5	104.25	58.7	67.2 5
5	89	96	116	125.3	85.9	93.8	61.9	70.7
6	88.65	95.75	114	123.5	96.9	105.8	69	78.3
7	83	90.35	114.2	123.65	84.25	93.25	54	63.3 5

9. $Mn = 80$, $\varphi = 30\%$

U _T	1		1.3		1.6		2	
P _{in}	1.56467		1.77146		1.97825		2.53964	
P _{out}	1.2545		1.392357		1.37857		1.413035	
Sample	P	T	P	T	P	T	P	T
0	112.55	116.1	135.1	139.3	137.95	141.3	93.3	96.5
1	106	111.1	124.65	131.25	125.45	131.65	92.7	99.1

2	105.95	111.8	128.5	136	127	135.2	87.6 5	95.9
3	99.4	109.3	122.6	133	122.35	135.1	93.9 5	106.3 5
4	108.7	119.1	127.5	139	120.05	133.45	80.6 5	94
5	104.4	114.9	123.95	137.4	121.7	135.3	79.5 5	93.75
6	108.85	120.3	122.4	137.1	121.8	136.3	86.8	101.2
7	96.1	107.7	120.8	136	121.05	136.3	77.6	92.4

10. $Mn = 100$, $\varphi = 10\%$

U_T	1		1.3		1.6		2	
P_{in}			1.80592		1.97825		2.116107	
P_{out}			1.2545		1.288964		1.130428	
Sample	P	T	P	T	P	T	P	T
0			92.25	95.4	91	95	53.8	56.8
1			82.2	85.95	86.55	91.15	54.8	58.55
2			86.2	90.25	88.95	94.1	64.5	68.9
3			86.9	91.95	87.8	94.1	55.3	60.4
4			91.05	96.25	88.4	94.9	53.4	59
5			89.9	95.15	90.25	96.8	54	59.7
6			89.3	94.6	86.5	93	54	59.8

7			91.2	96.4	89.8	96.4	53.4	59.3
---	--	--	------	------	------	------	------	------

11. $Mn = 100$, $\varphi = 20\%$

U_T	1		1.3		1.6		2	
P_{in}	1.612928571		1.70253		1.874857		2.25396	
P_{out}	1.27517		1.2545		1.261392		1.357892	
Sample	P	T	P	T	P	T	P	T
0	138.1	142.55	100	103.5	93.6	96.6	71.1	75.4
1	146.55	151.8	105	110	70.8	75.5	74.6	80.7
2	149.1	154.6	107.75	113.6	65.5	71.55	70.75	78.4
3	142.75	150	97.2	104.9	65.1	73.85	68.3	78
4	148.3	156	104.15	113.45	64.25	73.45	68.6	79.2
5	143.4	152.2	93.75	103.75	64	73.6	70	80.65
6	131.4	140.85	93.4	103.7	63	73.15	69.9	80.6
7	132.35	141.75	96.05	106.75	63.2	73.5	69	79.8

12. $Mn = 100$, $\varphi = 30\%$

U_T	1		1.3		1.6		2	
P_{in}	1.56467		1.77146		1.84039		2.116107	
P_{out}	1.2545		1.37116		1.2889		1.344107	
Sample	P	T	P	T	P	T	P	T
0	94.15	97	121.55	125	121.6	126.8	88.8	93.8

1	94.65	100.65	117.2	123.1	118.2	126.6	79.7 5	88.2
2	87	93.5	113.05	120.7	117.85	128.5	76.9	88.6
3	92.6	102.25	106.9	117.9	97.4	113	66.2 5	82
4	91.75	101.9	110.7	124.3	110.8	126.8	67	84
5	85.7	96	105	119.3	99.9	117	62.5	80
6	89.5	100.5	110.2	125	110.2	128	70.2	87.5
7	87.5	100.6	96.75	111.9	104.3	122	65.5	82.7

APPENDIX III

SAMPLE CALCULATION

A sample calculation for computing k_{La} is provided in this section. The chosen experimental run has the following conditions:

Table 5: Experimental Conditions

Condition	Value
Mesh Number	50
Number of screen elements	15
Inter screen spacing (mm)	40
Screen open area (%)	30.25
Dispersed phase holdup (%)	30
Water flow rate, Q_L , (L/min)	41.2
Gas flow rate, Q_g , (L/min)	17.6625
CO ₂ flow rate, Q_g (L/min)	5.29875
Air flow rate, Q_g (L/min)	12.36375
Temperature (K)	295

As previously mentioned k_{La} is obtained from plotting $\ln(C_{CO_2}^* - C)$ versus t . Therefore, t , $C_{CO_2}^*$ and C should be calculated first.

The residence time is calculated using the total superficial velocity,

$$t = \frac{d}{U_T} \quad [19]$$

Where U_T is determined from the gas and liquid flow rates as shown below:

$$U_T (m/s) = \frac{Q_L + Q_g}{1000 \times 60 \times A_c} = 2 \quad [20]$$

and A_c is the cross-section area of the column and is equal to:

$$A_c = \frac{\pi D^2}{4} = \frac{\pi(0.025^2)}{4} = 4.90625 \times 10^{-4} m^2 \quad [21]$$

C , the concentration of CO_2 in the liquid phase in the form of CO_3^{2-} , is calculated according to Warder and Winkler's method. For example, at sample 2

$$C \left(\frac{mol}{L} \right) = \frac{(T - P) \cdot C_{acid}}{v_{sample}} \quad [22]$$

P (mL)	T (mL)	Acid Concentration (M)	C (M)
78	85.4	0.00965	0.001544

To calculate $C_{CO_2}^*$, knowledge of the local partial pressure of CO_2 is needed and obtained by assuming that $\frac{\Delta P}{\text{Length of the reactor}}$ is constant for each experiment. Therefore, the local pressure at each sampling point is calculated from the following equation

$$P_x = P_{bottom} - \frac{\Delta P}{\text{Length of the reactor}} \cdot X$$

Where X = length from the pressure sensor at the bottom of the reactor to the sampling point;

m

For example, $\frac{\Delta P}{\text{Length of the reactor}} = 0.007232367 \text{ atm/cm}$ and $P_{bottom} = 2.156462585 \text{ atm}$. At

sampling point 2 (x = 28 cm), $P_{x=28 \text{ cm}} = 1.953956319 \text{ atm}$.

Then, the local partial pressure of CO₂ at this point is

$$P_{CO_2} = P_x \cdot y$$

Where y = local mole fraction of CO₂

The last step in determining $C_{CO_2}^*$ is to calculate it from Henry's law which is calculated according to equation [9-12] found in the methodology section.

Henry's law of CO₂ in water is calculated according to equation 10 and is 0.03150141 kmol/(m³.bar). Then, Henry's constant in an electrolyte solution is calculated using equation [9-12] according to the values found in

Table 6.

Table 6: Ionic strength calculation

Ions	Concentration of Ions (M)	Ionic Strength
Na ⁺	0.13373	0.13373

K^+	0.0000375	0.0000375
OH^-	0.008456646	-0.008456646
CO_3^{2-}	0.004688833	-0.009377667

Therefore, the Henry's constant of CO_2 in an electrolyte solution turns out to be 0.030684063 kmol/(m³.bar).

Similarly, the same is done for all other samples. As such, the table below is obtained:

Samples	x (cm)	t (s)	C (M)	$C_{CO_2}^*$ (M)	$\ln (C_{CO_2}^* - C)$
Control Sample	0	0	0	0.058823	-2.83322
1	18	0.09	0.00072375	0.054761	-2.91808
2	28	0.14	0.001544	0.052478	-2.97723
3	38	0.19	0.00400475	0.0502	-3.07487
4	48	0.24	0.0043425	0.047938	-3.13281
5	58	0.29	0.005211	0.045688	-3.20701
6	68	0.34	0.005621125	0.043416	-3.27558
7	78	0.39	0.005572875	0.041183	-3.33513

The following plot is obtained:

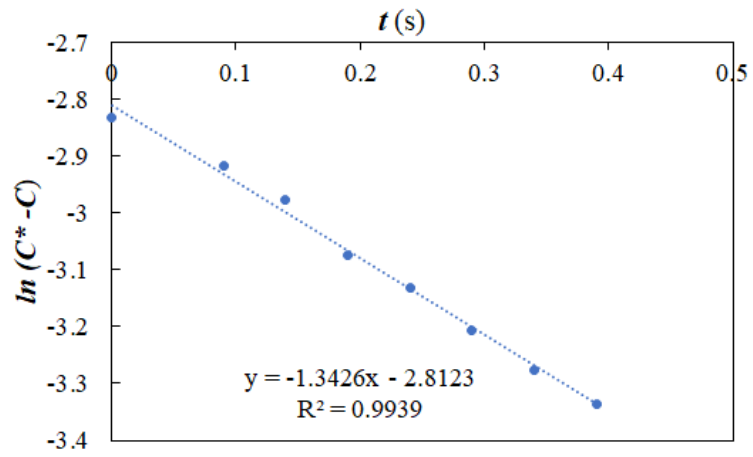


Figure 18: k_{LA} calculation

APPENDIX IV

ERROR ANALYSIS

In this investigation, the physical quantities directly measured are subject to errors associated with the instruments used.

The following table presents the errors associated with each measured physical quantity.

Table 7: Errors associated with the physical quantities

Physical quantity measured	Error
Q_L	5%
Q_g	4%
Volume in burette	0.05 mL
Pressure transducer	0.4 kPa

To calculate the propagated error on the evaluation parameter, the following equation was used.

$$\Delta y_i = y(x_1, x_2, \dots, x_i + \Delta x_i, \dots, x_n) - y(x_1, x_2, \dots, x_n) \quad [23]$$

1. Error on $\frac{\Delta P}{screen}$ (kPa):

$$Error\ on\ \frac{\Delta P}{screen}\ (kPa) = \frac{\Delta P_{bottom} - \Delta P_{top}}{15} = \frac{0.4 + 0.4}{15} = 0.05333 \quad [24]$$

2. Error on U_T (m/s):

The error on U_T is given by the following equation

$$\Delta U_T\ (m/s) = \Delta U_L + \Delta U_g \quad [25]$$

Sample calculation:

Table 8: Sample calculation of the error on $U_T = 2$ m/s

U_{gas} (m/s)	ΔU_{gas} (m/s)	U_L (m/s)	ΔU_L (m/s)	ΔU_T (m/s)
0.6	0.024	1.4	0.07	0.094

3. Error on φ

The error on φ is obtained by the error on U_g and U_L and is represented by the following formula

$$\Delta\varphi = \left(\frac{U_g + \Delta U_g}{U_L + \Delta U_L + U_g + \Delta U_g} - \frac{U_g}{U_L + U_g} \right) \quad [26]$$

Table 9: Sample calculation of the error on φ for the condition $Mn = 30$, 1m/s & 20% Holdup

φ	U_g (m/s)	U_L (m/s)	U_T (m/s)	ΔU_g (m/s)	ΔU_L (m/s)	ΔU_T (m/s)	$\Delta\varphi$
0.1	0.1	0.9	1	0.004	0.045	0.049	0.00085796
0.2	0.2	0.8	1	0.008	0.04	0.048	0.001526718
0.3	0.3	0.7	1	0.012	0.035	0.047	0.002005731
0.1	0.13	1.17	1.3	0.0052	0.0585	0.0637	0.00085796
0.2	0.26	1.04	1.3	0.0104	0.052	0.0624	0.001526718
0.3	0.39	0.91	1.3	0.0156	0.0455	0.0611	0.002005731

0.1	0.16	1.44	1.6	0.0064	0.072	0.0784	0.00085796
0.2	0.32	1.28	1.6	0.0128	0.064	0.0768	0.001526718
0.3	0.48	1.12	1.6	0.0192	0.056	0.0752	0.002005731
0.1	0.2	1.8	2	0.008	0.09	0.098	0.00085796

4. Error on time

From ΔU_T the error on residence time (Δt) can be calculated as shown below:

$$\Delta t (s) = t - \frac{d}{U_T + \Delta U_T} \quad [27]$$

$$\% \text{ error } (\Delta t) = \frac{\Delta t}{t} \times 100 \quad [28]$$

Table 10: Calculation of the error on t for the condition Mn = 30, 1m/s & 20% Holdup

U_T (m/s)	ΔU_T (m/s)	t (s)	Δt (s)	Δt (%)
1	0.049	0.6	0.028027	4.671115
1	0.048	0.6	0.027481	4.580153
1	0.047	0.6	0.026934	4.489016
1.3	0.0637	0.461538	0.021559	4.671115
1.3	0.0624	0.461538	0.021139	4.580153
1.3	0.0611	0.461538	0.020719	4.489016
1.6	0.0784	0.375	0.017517	4.671115
1.6	0.0768	0.375	0.017176	4.580153
1.6	0.0752	0.375	0.016834	4.489016

2	0.098	0.3	0.014013	4.671115
2	0.096	0.3	0.01374	4.580153
2	0.094	0.3	0.013467	4.489016

5. Error on $[CO_3^{2-}]$

The error on the $[CO_3^{2-}]$ propagates from the volume read from the burette. Therefore,

$$[CO_3^{2-}]_{(e)} = \frac{C_a \cdot (T - P + \Delta V)}{V_{sample}} \quad [29]$$

Where, $[CO_3^{2-}]_{(e)}$ = concentration of CO_3^{2-} including the error in reading the burette; M

ΔV = error in reading the volume from the burette; mL

C_a = concentration of the acid; M

V_{sample} = volume of the sample; mL

The error would be then:

$$\% \text{ error } [CO_3^{2-}] = \frac{[CO_3^{2-}]_{(e)} - [CO_3^{2-}]}{[CO_3^{2-}]} \times 100 \quad [30]$$

Table 11: Estimation of the % error on Efficiency for the condition Mn = 30, 1m/s & 20%

Holdup

U_L (m/s)	ΔU_L (m/s)	$[CO_3^{2-}]$ (M)	$[CO_3^{2-}]_{(e)}$ (M)	Efficiency (%)	Efficiency with the error (%)	% Error in Efficiency (%)
0.8	0.84	0.000165113	0.000192631	4.93136	5.753253333	16
0.8	0.84	0.000275188	0.000302706	8.218933333	9.040826667	10
0.8	0.84	0.000825563	0.000853081	24.6568	25.47869333	3
0.8	0.84	0.001265863	0.001293381	37.80709333	38.62898667	2.2
0.8	0.84	0.001155788	0.001183306	34.51952	35.34141333	2.38
0.8	0.84	0.001843756	0.001871275	55.06685333	55.88874667	1.49
0.8	0.84	0.001926313	0.001953831	57.53253333	58.35442667	1.42

6. Error on $k_L a$

The error on $k_L a$ is computed by the following formula:

$$\% \text{ error } (k_L a) = \frac{k_L a_{(e)} - k_L a}{k_L a} \times 100 \quad [31]$$

$k_L a_{(e)}$ is the slope of the plot $\ln(C_{CO_2}^* - C)$ vs t_e .

Therefore, for the condition $Mn = 30$, 1m/s & 20% holdup, $k_L a_{(e)}$ is 0.242 s^{-1} . Therefore, the error on $k_L a$ is 2.77% .

7. Error on E_{spm}

The E_{spm} for the specified experimental run is $0.007655952\text{ kWh/tonne}$.

The error on E_{spm} was calculated by determining ΔE_{spm} as shown below:

$$\begin{aligned} \Delta E_{spm}(\text{kWh/tonne}) & \quad [32] \\ & = E_{spm} - \frac{(\Delta P + 0.0533) \cdot (Q_L + \Delta Q_L + Q_G + \Delta Q_G)}{V \cdot \rho_{mix}} \times (t + \Delta t) \\ & = 0.007674196\text{ kW.h/tonne} \end{aligned}$$

The percentage error on E_{spm} is calculated as follows:

$$\% \text{ error } (E_{spm}) = \frac{\Delta E_{spm}}{E_{spm}} \times 100 = 0.238\% \quad [33]$$

8. Error on Re

The error propagation on Reynolds number was also calculated for the specified experimental run. All Reynolds numbers, Re , Re_b , Re_M , Re_j and Re_{jet} , are dependent on U_T . So, they are affected by ΔU_T .

Table 12: Estimation of the % error on Reynolds number for the condition Mn = 30, 1m/s & 20% Holdup

	Value	Value (w/error)	% error
Re	24901.07893	26096.33072	8.05
Re _b	303.5939543	318.1664641	4.799
Re _M	834.8833743	874.9577763	4.8
Re _j	1480.612174	1551.681558	4.7997
Re _{jet}	61484.1455	64435.38449	4.8

9. Error on Efficiency

The error on efficiency was also calculated for the specified experimental conditions and is dependent on U_L and $[CO_3^{2-}]$.

Table 13: Estimation of the % error on Efficiency for the condition Mn = 30, 1m/s & 20% Holdup

U_L	ΔU_L (m/s)	$[CO_3^{2-}]$ (M)	$[CO_3^{2-}]_{(e)}$ (M)	% error $[CO_3^{2-}]$
1.8625	2.09625	0.000165113	0.000192631	16
1.59125	1.84625	0.000275188	0.000302706	10
1.54375	1.79375	0.000825563	0.000853081	3
1.5375	1.825	0.001265863	0.001293381	2.2

1.47375	1.81875	0.001155788	0.001183306	2.38
1.46875	1.8175	0.001843756	0.001871275	1.49
1.46	1.81	0.001926313	0.001953831	1.42
